SURFACE MODIFICATION OF TI-ALLOY WITH SILVER SILICON NITRIDE COATING FOR ANTIBACTERIAL APPLICATIONS

UMI ZALILAH MOHAMAD ZAIDI

ENGINEERING FACULTY
UNIVERSITY OF MALAYA
KUALA LUMPUR

2019

SURFACE MODIFICATION OF TI-ALLOY WITH SILVER SILICON NITRIDE COATING FOR ANTIBACTERIAL APPLICATIONS

UMI ZALILAH MOHAMAD ZAIDI

DISSERTATION SUBMITTED IN FULFILMENT OF THE REQUIREMENTS FOR THE DEGREE OF MASTER OF ENGINEERING SCIENCE

ENGINEERING FACULTY
UNIVERSITY OF MALAYA
KUALA LUMPUR

2019

UNIVERSITY OF MALAYA

ORIGINAL LITERARY WORK DECLARATION

Name of Candidate: (I.C/Passport No:)

Matric No:

Name of Degree:

Title of Dissertation:

Field of Study:

I do solemnly and sincerely declare that:

(1) I am the sole author/writer of this Work;
(2) This Work is original;
(3) Any use of any work in which copyright exists was done by way of fair dealing and for permitted purposes and any excerpt or extract from, or reference to or reproduction of any copyright work has been disclosed expressly and sufficiently and the title of the Work and its authorship have been acknowledged in this Work;
(4) I do not have any actual knowledge nor do I ought reasonably to know that the making of this work constitutes an infringement of any copyright work;
(5) I hereby assign all and every rights in the copyright to this Work to the University of Malaya ("UM"), who henceforth shall be owner of the copyright in this Work and that any reproduction or use in any form or by any means whatsoever is prohibited without the written consent of UM having been first had and obtained;
(6) I am fully aware that if in the course of making this Work I have infringed any copyright whether intentionally or otherwise, I may be subject to legal action or any other action as may be determined by UM.

Candidate's Signature Date:

Subscribed and solemnly declared before,

Witness's Signature Date:

Name:

Designation:

ABSTRACT

Ti64 alloys is an alpha-beta titanium alloy with good corrosion resistance, high strength-to-weight ratio, excellent physiochemical stability, mechanical integrity and good biocompatibility. Ti64 alloy is the most promising biomaterials started to replace both stainless steel and cobalt-based alloys in many medical applications such as in orthopedics, dental areas and others. However, Ti64 alloy loses its biocompatibility when it is introduced into human tissues due to possible toxic of Vanadium (V) and Aluminum (Al) release. Releasing of these ions could cause many health problems like Neuropathy, Alzheimer and Osteomalacia. Therefore, to overcome the problem, surface modification using silver silicon nitride film via magnetron sputtering technique was proposed. Silver was proven to have an antibacterial function while silicon nitride is a biocompatible material with low wear rate. The AgSiN thin film is aimed to improve the biocompatibility and mechanical performance of Ti64 alloy by reducing the releasing of V and Al ions caused by debris or wear as well as providing antibacterial properties through the releasing of silver ions in an aqueous environment. Among the deposition parameters such as DC-RF power, temperature, gas flow rate and deposition time, substrate bias is considered as an effective way to control the thin film microstructure and its properties. In this study, a set of experimental depositing AgSiN films on Ti64 alloy using different bias voltage (0, -75, -150 and -200 V) were fabricated. The surface characterization and mechanical performance of the thin film with respect to bias voltage were studied using scanning electron microscope (SEM), atomic force microscope (AFM), X-ray diffraction (XRD), X-ray spectroscopy (XPS), nanoindentation, scratch test and wear test. Crystallite size and microstrain of the films were determined using Approximation Method to further understand the deposited films. Meanwhile, the biological function of the films was tested through wettability and antibacterial tests. According to the results, all thin films showed similar morphology with the highest

adhesion strength (596 mN) of the AgSiN film was obtained for sample deposited at -75 V. In terms of hardness (5.5 GPa) and elastic modulus (211.0 GPa), sample deposited at -150 V showed an improvement for about 50% compared to the Ti64 substrate (H=2.75, E=113.8). Microstrain values acquired from the Approximation Method were used to project the residual stress present in the film where the lowest compressive residual stress (0.06 GPa) was noted for samples that have highest adhesion strength and highest thickness. In terms of biological functionality, all films showed hydrophilic property with wetting angle observed were below 90º. An inhibition zone area that observed on *Bulkholderia pseudomallei (B.Pseudomallei)* and *Escherichia coli (E.coli)* were 7 and 10 mm, respectively which proved the AgSiN films as a promising candidate to be used in antibacterial applications.

Keywords: Surface Modification, Titanium alloy, Silver silicon nitride, Magnetron sputtering, Antibacterial applications.

ABSTRAK

Ti64 merupakan alpha-beta titanium aloi yang mempunyai rintangan kakisan yang baik, nisbah kekuatan-berat-tinggi, kestabilan fisiologi kimia yang baik intergriti mekanikal dan serasi yang baik. Alatan Ti64 adalah biomaterial yang mula menggantikan kedua-dua keluli tahan karat dan aloi berasaskan kobalt dalam pelbagai aplikasi perubatan seperti ortopedik, kawasan pergigian dan lain-lain. Walau bagaimanapun, apabila aloi Ti64 diperkenalkan ke dalam tisu manusia, kemungkinan pelepasan bahan toksik seperti Vanadium (V) dan Aluminium (Al) menyebabkan Ti64 aloi kehilangan keserasian. Pelepasan ion-ion ini boleh menyebabkan masalah kesihatan seperti penyakit saraf, demensia dan osteomalasia. Oleh itu, bagi mengatasi masalah tersebut, pengubahsuaian permukaan menggunakan filem silikon nitrida perak melalui teknik percitan magnetron telah dicadangkan. Komponen perak telah dibuktikan mempunyai fungsi antibakteria manakala silikon nitrida pula adalah bahan serasi dan mempunyai kadar haus yang rendah. Filem nipis AgSiN ini bertujuan meningkatkan keserasian dan prestasi mekanikal aloi Ti64 dengan cara mengurangkan pembebasan ion V dan Al yang berpunca daripada serpihan serta menyediakan sifat antibakteria melalui pelepasan ion perak dalam persekitaran yang berair. Antara parameter pemendapan seperti kuasa DC-RF, suhu, kadar aliran gas dan masa pemendapan, kecenderungan substrat dianggap sebagai cara yang berkesan untuk mengawal mikrostruktur filem tipis dan sifatnya. Dalam kajian ini, satu set percubaan mendepositkan filem AgSiN pada aloi Ti64 menggunakan voltan bias yang berbeza (0, -75, -150 dan -200 V) telah dilakukan. Pencirian permukaan dan prestasi mekanikal filem nipis yang berkaitan dengan voltan bias telah dikaji dengan menggunakan mikroskop elektron pengimbasan (SEM), mikroskop berkuatkuasa atom (AFM), X-ray difraksi (XRD), X-ray spectroskopi (XPS), nanoindentasi, ujian calar dan ujian kelusuhan. Saiz kristal dan mikroterikan filem-filem telah ditentukan dengan menggunakan Kaedah Penghampiran dimana teknik ini digunakan untuk lebih

memahami sifat filem. Sementara itu, fungsi biologi filem diuji melalui kebolehkerjaan dan ujian antibakteria. Berdasarkan keputusan yang diperoleh, semua filem nipis menunjukkan morfologi yang sama dengan kekuatan melekat tertinggi (596 mN) daripada filem AgSiN yang diperolehi untuk sampel yang disimpan di -75 V. Dari segi kekerasan (5.5 GPa) dan modulus elastik (211.0 GPa), sampel didepositkan pada -150 V menunjukkan peningkatan kira-kira 50% berbanding dengan substrat Ti64 (H = 2.75, E = 113.8). Nilai mikroterikan yang diperoleh daripada Kaedah Penghampiran telah digunakan untuk mengira tekanan sisa di dalam filem di mana kekuatan mampat terendah (0.06 GPa) telah diperhatikan untuk sampel yang mempunyai tahap kekuatan lekatan tertinggi dan ketebalan yang tinggi. Dari segi fungsi biologi, semua filem menunjukkan sifat hidrofilik dengan sudut pembasahan yang diperhatikan berada di bawah 90º. Kawasan zon perencatan yang dilihat pada *Bulkholderia pseudomallei (B.Pseudomallei)* dan *Escherichia coli (E.coli)* masing-masing adalah 7 dan 10 mm yang membuktikan filem-filem AgSiN sebagai calon yang menjanjikan untuk digunakan dalam aplikasi antibakteria.

Keywords: Modifikasi permukaan, Titanium aloi, Perak silicon nitrida, Kaedah pemercitan, Aplikasi antibakteria.

ACKNOWLEDGEMENTS

In the name of Allah, The Most Gracious and The Most Merciful, Praise to Him the Almighty that His will and given strength the author succeeds to finish and complete the thesis.

The author would like to thank to **Dr. Reza Mahmoodian** and **Assoc. Prof. Dr.Ir Bushroa Abdul Razak** for guidance throughout the thesis preparation. The author would also thank to **Dr.Kumutha** from the Microbiology Laboratory Department, University Malaya Medical Centre (UMMC) for her help in antibacterial test.

The author would also express her appreciation to the Surface Lab technician, **Mrs. Hartini** who endlessly giving help and explanation in the lab. **Mr. Zaharudin**, technician in Geology Faculty who taught the author on XRD analysis as well as friends who are giving moral support throughout this master journey.

The authors would also gratefully acknowledge the University of Malaya for the financial support given under a grant (PG185-2016A).

Finally, the author would like to thank to her support and understanding parents **Pn. Omi Kelsom Saidin** and **En.Mohamad Zaidi Zain** and other family members; **Zamin, Zakuan and Zakirah**. Their encouragements and advices when the times got rough were truly appreciated.

TABLE OF CONTENTS

LIST OF FIGURES

LIST OF TABLES

LIST OF SYMBOLS AND ABBREVIATIONS

V	Vanadium
Al	Aluminum
AgSiN	Silver silicon nitride
SEM	Scanning electron microscope
EDS	Electron dispersive spectroscopy
AFM	Atomic force microscope
XRD	X-ray diffraction
XPS	X-ray photoelectron spectroscopy
ºC	Degree Celsius
DC	Direct current
RF	Radio frequency
Ar	Argon
N	Nitrogen
Ag	Silver
Ti	Titanium
EDM	Electron discharge machine
ICSD	International centre for diffraction data
W-H	Williamson-Hall
W-A	Warren- Averbach
Pa	Pascal
µm	Micron-meter
V	Volt
Lc	Critical load

COF	Coefficient of friction
%	Percentage
T	Temperature
µl	Micro-litre
º	Degree
E.coli	Escherichia coli
B.psudomallei	Bulkholderia pseudomallei
Nm	Nanometers
B	Broadening
M	Particle size broadening
N	Strain broadening
M(2θ)	Profile broadening function
N(2θ)	Strain broadening function
FWHM	Full width at half maximum
D	Crystallite size
E	Strain
E	Elastic modulus
Σ	Stress
H	Hardness
Dc	Critical distance
T	Thickness
CAZ	Ceftazidime
DOX	Doxycycline
TGC	Tigecycline

CHAPTER 1: INTRODUCTION

1.1 Introduction

This study investigates the properties of the AgSiN coating deposited on the biomaterial Ti64 alloy for the antibacterial applications which is relatively unexplored in the literature. This chapter sets the background and introduction of the research study. The chapter also provides an overview of the subsequent chapters of this thesis.

This chapter is organized as follows. Section 1.2 provides the background of the study. Section 1.3 explains the motivation of the undertaking research which include the knowledge gap and the potential benefits. Section 1.4 states the objectives of the research followed by Section 1.5 which presents the thesis outline.

1.2 Background of study

Technology has been driving the evolution in biomedical research by improving the medical tools as well as aided in the disease treatment. A field that has become closely associated in this medical discipline is mechanical engineering. The continuous progress between the engineering and medical science make the gap exists between those two grows even thinner. Examples are such as biosensors, biomaterials, artificial system and other medical devices.

Biomaterials are any material that have been engineered to interact with the biological system. Meanwhile, biocompatibility is related to the behavior of the biomaterials react to an organism's immune response. Excellent biocompatibility means the material elicit no or less when it is in contact or being implanted in an organism (Anderson, 2011). Biomaterials can be classified as bio-metals, bio-ceramics, bio-composite and bio-polymers.

Bio-metals were first introduced as metal plate for bone fixation in 1895 by Lane, (Lane, 1895) 100 years ago. In its early development, the bio-metals experienced insufficient strength and corrosion problems. Thereafter, metal implants immediately attracted clinician's interest and experienced endless development and clinical use. Meanwhile, bio-composite consists of biodegradable polymer and bio-fibers as matrix and reinforcing elements respectively. Bio-composites are known for its low density, good thermal properties, high toughness, ease of separation, enhanced energy recovery, biodegradability and generally low cost (Reddy, Kim, & Park, 2016). For instance, nano-hydroxyapatite has been used for dental/orthopedic implants due to its similar structure and chemical compositions to the human bone (R. Ma et al., 2014).

Another subset of biomaterials is bio-ceramics. Bio-ceramics have wide range of biocompatibility where they are inert in the body. In an extreme case, after the bio-ceramics assisted a repair, the material eventually replaced by the body. Bio-polymers are polymers that produced by living organism. Cellulose and starch, protein and peptides and DNA and RNA are examples of bio-polymers. The applications of bio-polymers are included in tissue engineering, post-surgical treatment, wound healing and controlled of releasing drugs (Nazari et al., 2017).

Three most used bio-metals in medical applications like implants and medical devices are cobalt-chromium (Co-Cr alloy), stainless steel (SS) and titanium (Ti) and its alloy. Stainless steel which is used for implants contains approximately 18 wt.% of Cr and around 8 w.t% of Ni which makes stainless steel resistant to corrosion and stronger compared to steel. Afterwards, improvements had been made by introducing the molybdenum (Mo) element into the stainless steel that enhanced further its' corrosion resistance. This steel is known as type 316 stainless steel. Next, researchers reduced the carbon (C) content from 0.08 to 0.03 w.t% and thus help the steel (named 316 L) to resist

corrosion from the chloride solution. As for Co-Cr alloys, it has been used as artificial joints for many decades thanks to their excellent wear resistance. Meanwhile, Ti and alloys, i.e. Ti64 alloy are known for its lightweight (4.5 g/cm^3), compared to 8.3 g/cm^3 for cast CoCrMo alloys and 7.9 g/cm^3 for 316 stainless steel (Brandes, Brook, & Paufler, 1993), has good pitting corrosion resistance and excellent tensile strength. Nitinol, a material where titanium alloyed with Ni is known to have shape memory effect, therefore make it suitable to be used in applications like dental restoration wiring. In the current study, researcher chose to use Ti64 alloy as the research material.

Ti64 alloys is an alpha-beta titanium alloy with good corrosion resistance, high strength-to-weight ratio, excellent physiochemical stability, mechanical integrity and good biocompatibility. Even though, the Ti64 alloy has many advantages, it also has drawbacks qualities, which include low wear resistance and low shear strength when it is used in orthopedic prostheses. Besides, releasing of Vanadium (V) and Aluminum (Al) ions from the alloy also has the possible toxic effect. Releasing of these ions can cause long term health problems such as neuropathy, Alzheimer and Osteomalacia (Geetha, Singh, Asokamani, & Gogia, 2009). To encounter and enhance the durability, functionality and biocompatibility of Ti64 alloy, different approach has been used. Such changes include modifying the material structure, surface roughness, surface chemistry, wettability, surface charge, surface energy and hardness. As V and Al are toxic elements, surface modification is regarded as one of the good methods to encounter this problem.

Various surface modifications have been introduced such as plasma spray coating, ion implantation (Vlcak, Cerny, Drahokoupil, Sepitka, & Tolde, 2015), chemical vapor deposition (X. Li et al., 2013) and thermo chemical surface modification like nitriding (Samanta et al., 2018), carburization and boriding (Qin, Liu, Yang, & Tang, 2013) . In this work, the Physical Vapor Deposition Magnetron Sputtering (PVDMS) method will

be used as a technique to improve the Ti64 alloy. Meanwhile, the combination of silver, silicon and nitrogen (AgSiN) is seen as the proper material to modify the alloy. In titanium alloy surface modifications, silver silicon nitride is not widely explored as thin films. Nevertheless, the combination of silver and silicon nitride as thin film system on Ti64 alloy could open up new surface modification as silicon nitride exhibit high hardness and wear resistance. Meanwhile, silver can act as lubricant and reduce the surface roughness in mechanical applications aside from having the antibacterial properties.

1.3 Motivation of the study

In this section, the author will discuss the factor that motivates the research taken in this study whereby sub-section 1.3.1 presented the knowledge gap and sub-section 1.3.2 will be elaborated on the potential benefit.

1.3.1 The knowledge gap

Ti64 alloy had been extensively used in many applications including biomedical devices thanks to its excellent and desirable properties such as biocompatibility, relatively low modulus, formability, machinability, good fatigue strength and corrosion resistance. However, the Ti64 alloy also has its drawbacks which are the possibility of toxic effect of the Al and V ions release, low shear strength and low wear resistance when it is used in orthopedic prostheses. Besides, Ti64 alloy also does not have antibacterial properties which make the alloy still not fulfilling the clinical requirement. In order to meet the clinical requirements, Ti64 surface is often modified to improve its mechanical, chemical and biological properties.

Various investigations had been done to improve the tribological behavior of the Ti64 alloy and at the same time maintaining the antibacterial properties. Prior research commonly incorporated silver with strong ceramic materials like oxide, nitrides, carbides, yttrium and niobium to provide good mechanical as well as antibacterial properties to the

Ti64 alloy. Nevertheless, up to the best knowledge, magnetron sputtered silver silicon nitride (AgSiN) thin films onto the Ti64 substrate for antibacterial applications has not been reported yet. Therefore, an opportunity exists to understand the AgSiN thin film system and its possibility to improve Ti64 surface as well as its applicability in antibacterial applications.

In magnetron sputtering deposition process, substrate bias voltage plays a significant role in producing a good quality of thin films. The bias voltage influences the energy of the incoming ion bombardments on the substrate (so on the growing films). As mentioned in the afore paragraph, magnetron sputtered AgSiN films onto Ti64 alloys has not been studied yet thus, far from elucidated the effect of substrate bias parameter on the thin films. In this study, the author investigated the influence of substrate bias on the AgSiN film properties which include the surface, mechanical and wettability. The study also covered the residual stress effect in thin films caused by the substrate bias.

1.3.2 Potential benefits

An investigation of AgSiN thin films deposition on biomaterial Ti64 alloy may provide twofold benefits. First, the benefit will accrue the researchers and developers of new medical devices and those who are responsible in producing them. These findings may be used by the researchers and developers in deciding if a particular functionality can be provided by the thin film and what limitations may apply in a given application. Moreover, this study will satisfy a deeper knowledge in the biomaterial surface whereby overall contributing to the medical devices thin film development progress as well as enable a paradigm shift in antibacterial coating engineering.

Secondly, in the long term, this study will become one way to improve the human quality of life. With an ageing population, the number of patients with dentition defect or loss is growing annually. In short term, the biomaterial surfaces which are placed in

contact with the biological systems must be biocompatible and free from infectious agents meanwhile long-term wear and toxicity must also be addressed in the long term. Consequently, the demand for the antibacterial thin film will also increase. Thus, hopefully this study will help to solve the problem by developing medical thin films that is reliable, durable and high quality that meets unique requirements hence increasing the quality of patient life.

Despite the challenge in developing and manufacturing thin films, the potential of the AgSiN thin films will hopefully drive the surface and coating technology forward as well as adding solutions to the emerging healthcare surface enhancement market. Considering the increasing regulatory hurdles in the 21st century, a detail study needs to be done before the thin film can be commercially introduced. While the AgSiN thin film is still considered to be immature in relation to other established medical thin films, advancements in the next few decades are projected to make this thin film commercially viable.

1.4 Research objectives

The objectives of the thesis are:

i. To fabricate the AgSiN thin films at different bias voltage of sputtering machine for antibacterial applications.
ii. To determine the crystallite size and microstrain values of AgSiN thin films via the Approximation Method.
iii. To perform the mechanical, wettability and antibacterial test for the AgSiN thin films.

1.5 Thesis outline

This thesis is divided into five chapters. The chapter begins with Chapter 1 which covers the background of study, motivation of the research, objectives as well as the thesis outline.

Next, Chapter 2 is the literature review. This chapter reviews the latest and successful surface modification on titanium alloy. This section also elaborates and discusses on the technique chosen to deposit AgSiN films, parameter selection and the properties of silver as the antibacterial agent.

Chapter 3 presents the sample preparation, deposition technique, analyze method, characterization and tests employed throughout the research study. Flow chart, graph, photographs and schematic diagrams are used to illustrate and describe the contents.

Chapter 4 is the main section where the author presents, analyzes, discusses and relates results obtained from the characterizations. The author investigates the deposited AgSiN thin films according to the objectives highlighted. The discussion covered the influence of bias voltage on the surface and mechanical properties of AgSiN films, determination of crystallite and microstrain using Approximation method as well as the wettability and ability of the AgSiN thin films to exhibit antibacterial properties.

Lastly, Chapter 5 concludes this thesis along with some recommendations and future work.

CHAPTER 2: LITERATURE REVIEW

2.1 Introduction

Titanium and its alloys are common and widely used in medical applications. They have excellent biocompatibility, good corrosion resistance and brilliant mechanical properties (Niinomi, 1998). The applications of titanium and its alloys includes artificial heart valves (Wilson, Courtman, Klement, Michael Lee, & Yeger, 1995), blood vessel stents (Z. Ma, Kotaki, Yong, He, & Ramakrishna, 2005) and replacement with implants like knee, hip and elbow (Rack & Qazi, 2006). Among titanium alloys, Ti64 alloy gains attention in medical applications. The only concern about Ti64 alloy is on the releasing Vanadium (V) and Aluminum (Al) elements in the body environment, which are toxic and carcinogenic to human cells (Catalani et al., 2013).

In order to overcome the drawbacks of Ti64 alloy, silicon nitride was chosen to coat the alloy. Silicon nitride is known as bio-ceramic that has great combination properties like low wear, high fracture toughness, strength, resistance to scratches and biocompatible to the human body (Lin et al., 2005; M. Pettersson et al., 2013; Susuki, Yamada, Uchiyama, & Niwa, 1980). As for silver, this material was chosen as one of the coating materials because of its good antibacterial properties (Ewald, Glückermann, Thull, & Gbureck, 2006; Perez-Diaz et al., 2015). Many demonstrations had proved that some form of silver are effective against burns (El-Feky, Sharaf, El Shafei, & Hegazy, 2017), severe chronic osteomyelitis, urinary tract infections and central venous catheter infections (Jansen, Rinck, Wolbring, Strohmeier, & Jahns, 1994). By combining the excellent properties of each coating materials, silver and silicon nitride were hope to enhance the properties of Ti64 alloy. These materials could also be considered as a coating material to be used in medical applications in the future.

PVD coating technology is considered as an appropriate coating technique to coat AgSiN on Ti64 alloy. Physical vapor deposition magnetron sputtering (PVDMS) is used in this study due to its ability to coat ceramics and metals on the substrate material (Rahmati, Sarhan, Basirun, & Abas, 2016). Silver and Silicon are sputtered at the same time with the nitrogen purged into the chamber. This is done to attain the AgSiN compositions during deposition.

In thin films fabrications, it is crucial to control the deposition parameters as it will control and influence the properties of thin films. There are several ways to improve the quality of the on growing thin films. One of the methods is to control the energetic ions species bombarding on the growing films. The ion bombardment contributes to the momentum and kinetic energy of the arriving thin film's atoms, thereby increase their mobility on the substrate's surface or the growing thin film which thus affects the thin film's coalescence, nucleation and growth. Besides, by increasing the energy at the arriving atoms and in their surface, mobility enables depositions at lower substrate temperature with dense film microstructure, selectable stress level and in some cases desired crystallographic phases. Furthermore, ion bombardment can reduce the film's impurity level by knocking off loosely attached impurity atoms reaching the deposited film surface. Reducing the impurity level in depositing films is very important, especially when it will be used in critical applications, e.g. medical applications (Ensinger, 1997).

In this study, the focus will be on fabricating AgSiN thin film on Ti64 alloy via DC-RF co-sputtering technique with a provision of substrate biasing.

2.2 Substrate and thin film materials

2.2.1 Ti-6Al-4V (Ti64)

The most widely used titanium alloy is Ti64, grade 5. Ti64 is a two phase $\alpha + \boldsymbol{\beta}$ titanium alloy, with aluminum as the alpha stabilizer and vanadium as the beta stabilizer.

Highlighted advantages of Ti64 alloy are good corrosion resistance (Schenk, 2001), low density, high strength to weight ratio, low elastic modulus, small thermal expansion, non-magnetic, good fatigue resistance as well as fabricability (Ratner, 2001).

Nevertheless, Ti64 alloy suffers from shear strength and poor surface wear properties in certain loading conditions. Thus, it is undesirable for Ti64 alloy to be used for bone screws or plates. The poor surface wear properties will tends to seize during the sliding contact with itself or other metals. Degradation of material and released ions are the most common consequences of the reaction between body fluids which resulting in several problems including inflammations and formation of foreign body giant cells. Besides, Ti64 alloy, which contains vanadium, had been reported to demonstrate cytotoxic outcomes when isolated. Therefore, controlling and protection of coating's implants or medical devices are basic and indispensable demands.

2.2.2 Silver

Historically, silver (Ag) was discovered for more than 200 years, being used and keep revolutionizing since then (Barillo & Marx, 2014). On the periodic table, Silver element is located in period 5, group 11 with an atomic weight of 107.8682 u. Generally, Silver has been used for many applications like currency (Mendoza-López, Pérez-Bueno, & Rodríguez-García, 2009), electrical (Karakas, 2002), water treatment (Lv et al., 2009), industries as well as medical applications (Sussman, Jayanti, Dair, & Casey, 2015) . Meanwhile, applications of silver in the medical sector are huge. The claim had been made mention that silver can treat more than 650 different diseases such as cancer, tuberculosis, HIV, Ebola, cholera, warts, Meniere Disease, typhus, bubonic plague, malaria, lupus, ringworm, prostates, acne, sinusitis, Hanta and hemorrhoids (Marx & Barillo, 2014; Wadhera & Fung, 2005).

Silver ions and silver compound are known to be effective against a broad range of bacterial and microorganisms. Today, silver ions are used to control the bacterial growth in a variety of medical applications. The widely accepted mechanisms which involving with the silver entering the cell and cause damage. Silver ions simply appears to be a particle of a certain size with a + 1 charge to the transmembrane. In normal cell environment, the silver ions could get access into the interior of the cells easily through the transmembrane protein. This transmembrane protein normally functions to transport the ions such as calcium and potassium through the cell. For instances, Enterococcus hirae transmembrane protein which functions to transport copper was observed transporting the silver ions across the cell. Although there are no specific silver transporters existed in the transmembrane, there are ways for silver to be transported across the cell. (Dakal, Kumar, Majumdar, & Yadav, 2016). Figure 2.1 showed the general sequences of silver ions in the cell.

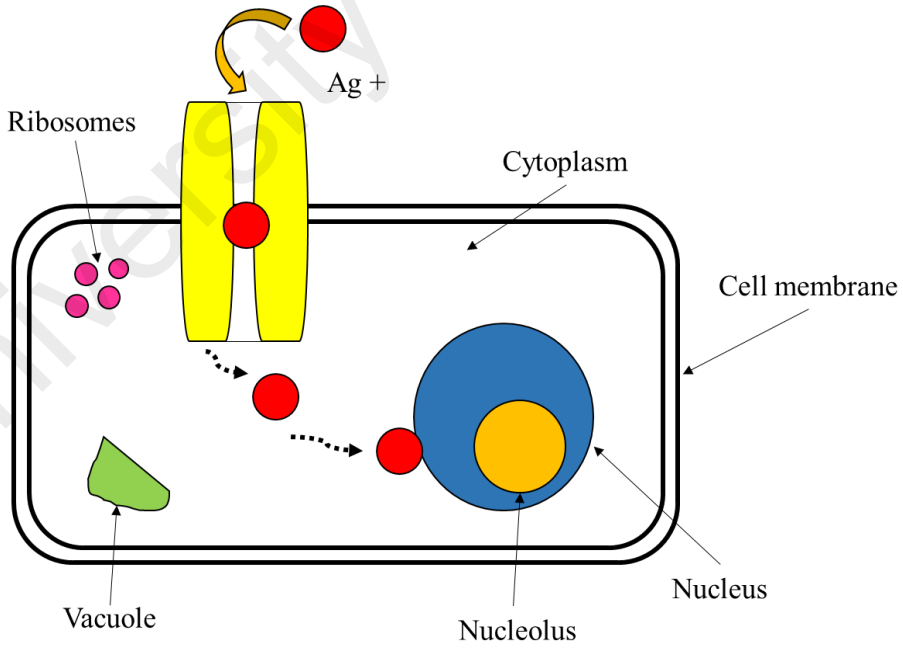

Figure 2.1. Antibacterial mechanism of Ag+ on bacteria cell.

It is believed that the silver ions attached to the ribosomes cause ribosome complex to deactivate and prevent the protein translations. In addition, bacterial growth that were

inhibit by the silver ions were then deposited as granules in the cell wall and vacuole. The silver ions damaged the cell envelope, cell division as well as the bacteria contents. Therefore, there will be abnormalities of the cytoplasmic membrane, bacterial cells, outer cell layers and the cytoplasmic contents. All these sequences will eventually lead to b cell death of the bacteria (W. K. Jung et al., 2008).

Due to this antibacterial ability, many researchers utilized the antibacterial surface fabrication. The modified surface becoming widely investigated and been used in various settings such as in clinics and at home. The most common use antibacterial coatings are in health care setting like sterilizations of medical devices to prevent hospital-associated infections. Antibacterial surface fabrication can be classified into several categories (refer Figure 2.2 which are i) bacteria attachment resistant surface, ii) surface treated with leaching antibacterial agents and iii) surface with contact-killing (Kaur & Liu, 2016).

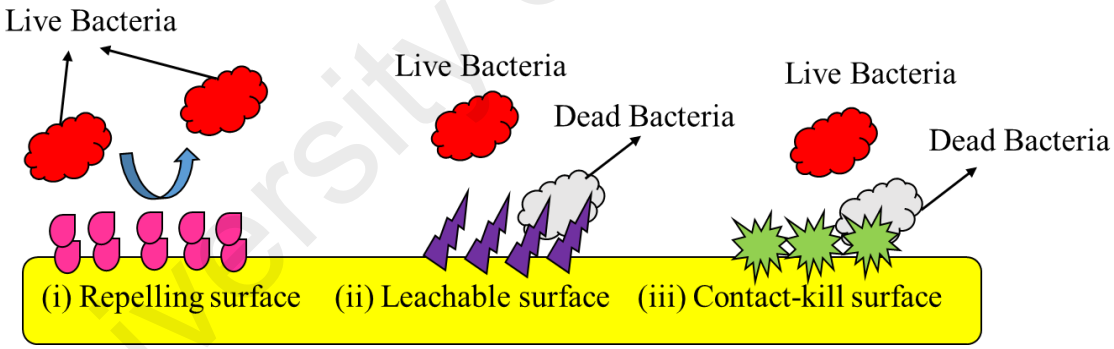

Figure 2.2.Categorization of antibacterial coating surface.

In the first approach, the surface is created so that it will resist bacterial adhesion instead of killing the bacteria. Ciston, Lueptow, and Gray (2008) and Whitehead and Verran (2006) have reported that hydrophobicity and surface roughness of coating's surface can attribute to the bacterial attachment resistance. In the second approach, the coating surface is usually incorporated with leaching agents like triclosan and silver. Their encapsulated biocides will leach out and kill the bacteria. However, the leached biocides

could get accumulated in the environment which make this approach unsustainable (Jeon, Yi, & Oh, 2003). Meanwhile, in the third approach, certain biocides are fixed into the contact-kill coating surface through covalent bonding whereby the bacteria will be killed when in contact with the surface (Kaur & Liu, 2016).

In order for silver to have antibacterial properties, the silver should be in its ionized form. This is because, silver is inert when it is in non-ionized form. But, when it is in contact with moisture, the silver will be ionized which lead to the releasing of silver ions (Melaiye & Youngs, 2005). Therefore, all forms of silver or silver containing compounds with observed antibacterial properties are from the silver ions (Ag^+). Silver ions can be released slowly with time by incorporating it into such as silver sulfadiazine (Venkataraman & Nagarsenker, 2013). Besides, silver ions can also be coming from the ionizing the silver solid surface such as with silver nanoparticles.

2.2.3 Silicon nitride

Silicon nitride has shown great combination of mechanical properties such as high fracture toughness, scratch resistance and low wear. These excellent properties cause Silicon nitride to be used widely in applications like ball bearings (Riley, 2000), cutting tool (W. Liu et al., 2016), optical applications as well as in medical applications (Matsunami et al., 2008).

In the last few decades, researchers emphasized on using oxide ceramics such as alumina and Zirconia to be used in implant and medical devices. Nevertheless, non-oxide ceramic like Silicon nitride also showed promising material as it has other good qualities beside mechanical properties including biocompatibility, bacterial adhesion resistance, hydrophilic behavior and radiographic imaging (Bock, McEntire et al. 2016). Silicon nitride surface texture and chemistry are highly tunable, yielding physicochemical combinations that may lead to enhanced osseointegration and bacterial resistance without

compromising bulk mechanical properties. In early 2011, the Food and Drug Administration (FDA) has approved the first implanted silicon nitride femoral head and a product silicon nitride based to be used as spinal implants in 2006 (Mantripragada, Lecka-Czernik, Ebraheim, & Jayasuriya, 2013) .

Many researchers utilized the excellent properties Silicon nitride as coating modification. Compared to the bulk ceramic or bulk metal, a ceramic coating on metal substrate could give a better performance as the wear resistance from the coating would be benefiting together with the substrate toughness. Furthermore, the ceramic coating can improve wear resistance and minimize metal ion release. Pettersson et al. (2016) had done a study which investigated the dissolution behavior of silicon nitride coatings for joint replacement. The result showed a low dissolution rate which is 0.2 – 1.4 nm/day and the dissolution rate of the coatings were similar to or lower than that CoCrMo (0.7 – 1.2 nm/day). The Silicon nitride coatings reduced the metal ions releasing from the substrate.

As an alternative to bulk silicon nitride, this study considered silicon nitride coatings that possess the above-mentioned potential advantages. Moreover, Silicon nitride coatings on metal offer a possibility to retain the benefit of a ductile bulk material and possibly avoid the risk of catastrophic fracture, which has been a concern for ceramics.

2.3 Physical vapor deposition (PVD) as the coating technique

Despite the excellent properties of Ti64 alloy such as corrosion resistance machinability, formability and biocompatibility, Ti64 still does not fulfill the clinical requirements like low shear strength and does not have the antibacterial properties. Therefore, one of the suggested techniques to enhance the properties such as mechanical properties and biological behavior is by surface modification. In this study the author utilized the PVD method to modify the Ti64 surface.

Physical Vapor Deposition (PVD) is a method used to deposit layers of material on the substrate. Thin film deposited typically in the range of several nanometers to few micrometers. PVD method is widely implement in various applications including in conductive coatings, microelectronics devices fabrications, optical, surface modifications and others. There are several different PVD technologies exist in the market. These PVD technologies commonly utilize the same three fundamental steps but different in terms of generate and deposition of material. Figure 2.3 shows the different PVD techniques that available in the market.

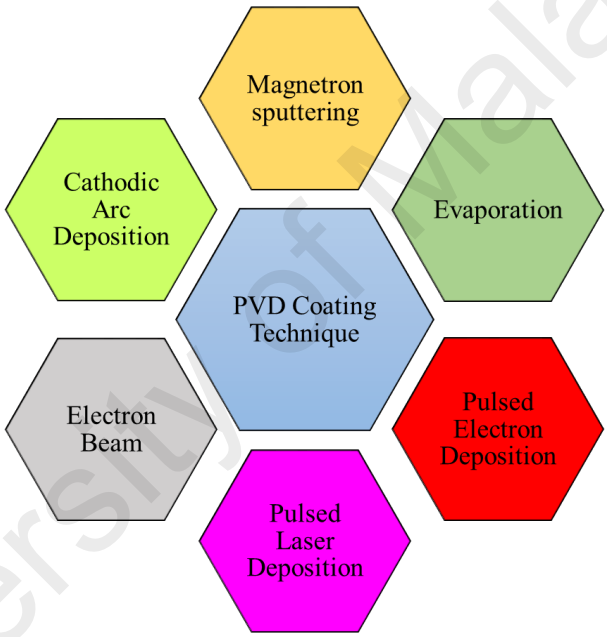

Figure 2.3. Various Physical Vapor Deposition method.

Among the PVD method, the author utilized the magnetron sputtering technique become the method of choice due to its high quality and well-adhered films. The magnetron sputtering process in vacuum condition has involved steps as follows, i) evaporation, ii) transport, iii) reaction and iv) deposition. At first place, the vacuum chamber was filled with inert gases such as Argon whereby the gas does not take part in the chemical reaction between target and substrate. Noted that the target is connected to the cathode while the substrate stage is connected to the anode. Once the Argon gas was

filled in, a high voltage between target and substrate was provided. The charge builds up near the cathode raise potential of plasma, which defined as the high temperature of ionize gas. Near the cathode area known as dark space zone, by which electrons move faster than Ar+ ions due smaller mass of electron. Ar gas atoms collide in-elastically with the high energetic electrons resulting in ionization of Argon gas (gas breakdown) rather than just excitation. The collisions between argon atom and electron charge produce ionize argon and two more electrons. The ionization of Argon gas is as follows.

$$Ar_2 \rightarrow 2Ar^+ + 2e^- \quad (1.1)$$

These Ar+ ions enter the dark space and accelerated towards the cathode (target). The bombarding Ar+ ions in the target cause the atoms to be locked out from the target and transport through the vacuum space directly to the anodic substrate. These releasing atoms will be deposited as a layer on a substrate as a result of the momentum transfer. This ejection process is known as sputtering. In reactive depositions, reactive gases are used such as nitrogen and oxygen. Mass flow controller is used to control the amount of gas that flows into the chamber. The ejected atoms can also possibly react with the appropriate gas (e.g. oxygen, nitrogen) if oxide or nitride coatings are desired. Sputtered atoms collide with substrate, form nucleation, island growth, coalescence and continuous growth. This eventually form an adhesive coating on the substrate (Mattox, 2002).

2.4 Depositions parameter affecting coating properties

In magnetron sputtering depositions, there are several parameters that can be varied in order to obtain a good quality of coatings. These parameters are base pressure, target power, gas flow, substrate-target distance, substrate rotation substrate temperature and substrate bias. Different deposition ‘recipe’ is needed when depositing different coating materials. Since there had been no research reported about AgSiN deposition on

biomaterial Ti64 alloy, the author uses the silver thin film deposition and silicon nitride thin film deposition from reported literatures as references.

Base pressure parameter is commonly related to the vacuum environment in the deposition chamber. A “good” environment provides a long mean free path for the collision between the vaporization source and the substrate. The good vacuum state also allows the user to control the vapor contamination and the amount of gas during the deposition process. Small change in the pressure at the start of a deposition can substantially affect the film interface chemistry and the adhesion strength of the film. If the intend work is nano-thin film (< 100 nm), the ideal deposition system is a system that can control the total base pressure as well as individual gas pressures before and during the deposition (Mattox, 2010).

Other deposition parameters are targets power. In the PVD system, a direct current (DC) and radio-frequency (RF) power supply can be connected to the target. Commonly, conductive target materials such as silver, steel and others are connected to the DC power supply meanwhile non-conductive target materials like silicon nitride, carbon and others are connected to the RF power. However, the connection can be changed depending on the desired coating properties. Dergez, Schneider, Bittner, Pawlak, and Schmid (2016) mentioned that in most scenarios, RF sputtered silicon nitride is a better choice. For instances, in MEM application devices, the Nevertheless, in some cases where low substrate surface and low impact energy are required, the RF sputtered silicon nitride is more suitable compared to the DC sputter deposition. The author also mentioned that, the material composition of the RF sputtered silicon nitride is strongly stoichiometric and towards the silicon rich compared to the close stoichiometric DC sputtered films. In the current research study, RF sputtering for silicon nitride had been chosen. This is due to the suitability of RF sputtering technique for all low process temperature applications and

at the same time and high deposition rate can be obtained although the silicon nitride is amorphous. (Vila, Prieto, García-López, & Respaldiza, 2003).

The gas flow parameter can be controlled by the mass flow controller (MFC). Yau and Huang (2004) reported the influence of nitrogen flow on silicon nitride films sputtered using RF power on high speed steel. The study showed that as nitrogen flow rate increase, the deposition rate is decrease. The reason could possibly due to the formation of compound on the target surface and a decrease in partial pressure of argon gas. The total electrons induced by the ionization in glow charger were decreased as the partial pressure of argon gas decreased. The decrease in electrons ionizing could eventually decreases the probability to dissociate nitrogen gas, which was probably the reason of decreasing of the amount of nitrogen species chemisorbed on silicon hence reducing the N/Si ratio. Besides, the hardness and elastic modulus of silicon nitride films decreases with flow rate of nitrogen gas because of the stoichiometric compositions.

Meanwhile, Khemasiri et al. (2015) investigated the effect of the Ar/N_2 gas timing ratio (10:0, 10:1, 10:3, 10:5, 10:7 and 10:10) on the compositions, morphology, hardness and corrosion resistance of silicon nitride thin film. Results revealed that, although the nitrogen content in the films increased only slightly when the N_2 timing was prolonged, the corrosion current of the film was decreased. A thin passivation oxidized layer was found to play a major role in the corrosion resistance. In contrast, the hardness properties exhibited a uniform variation with the N_2 timing. The gas timing sequence might induce morphological changes the underlying silicon nitride films. The high hardness obtained by the gas timing technique almost doubled that produced by the conventional mixed gas sputtering.

Substrate-target distance has pronounced by Asanithi, Chaiyakun, and Limsuwan (2012) to have an effect on the grain size of silver nanoparticles. According to the works,

at target-substrate distance of 20 cm, the smallest grain size (3.8 ± 0.7 nm) was obtained. Meanwhile, the target to substrate distance at 10 and 15 the silver nanoparticle obtained were 5.9 ± 1.8 and 5.4 ± 1.3 respectively. Increase in the silver nanoparticle size when decreasing the target-substrate distance has probably resulted from the increase in total amount of silver deposited. For example, the shorter the target-substrate distance, the higher the total amount of deposited silver and thus the larger the silver nanoparticle size will be. In this paper, it is suggested that the optimum target-substrate distance for synthesizing silver nanoparticles of uniform size is 20 cm.

Substrate rotation can also give an effect on the coating properties. During the deposition, it is a common practice that the substrate on the working table are kept rotated in order to achieve uniform deposition over the substrate surface. It was reported in Panich and Sun (2006) which coated TiB2 mentioned that the substrate rotation could affect the structure, orientation and hardness. According to Panich and Sun (2006), without substrate rotation, the resultant coatings of TiB2 exhibited the beneficial (001) orientation, dense and equiaxed grain structure which enhanced the hardness and adhesion strength. As the substrate rotates, the deposition rate was reduced as a result of reduced flux of adatoms. This would allow more time for the surface species to diffuse and thus favor the formation of a denser structure and development of the preferred texture. Second is the energy of the sputtered species arriving on the substrate surface. The energy of the sputtered species arriving on the stationary substrates is higher compared to the sputtered species arriving on the rotating substrates. Therefore, this would lead to an increase of adatom mobility and development of the preferred orientation and a denser structure in the coating.

Substrate temperature parameter could also alter the thin films properties. According to Hänninen (2018) increasing substrate temperature during deposition could result in

larger films stresses and slightly higher hardness. Meanwhile, in a study by Shah, Jayaganthan, and Kaur (2011), the deposition at low substrate temperature of the environment exhibits low adatoms and tends to form preferred crystal structure which lead to the increase in surface roughness. The reasoning is because the substrate temperature controls the adatoms on the surface mobility. The author also mentioned that as temperature increases from 100 to 500 ºC, the adatoms gains extra thermal energies and force to move to another preferred sites, which occurs in a random distributed manner due to free atomic motion. This is because the adatoms has higher probability to desorb from the surface at high substrate temperature.

Apart from that, the substrate bias voltage also is considered as a critical parameter in influencing the thin film properties. This is because the substrate bias voltage allows or control the ion bombardment energy on the substrate (so on the growing film). For example, in a study by the author Bait, Azzouz, Madaoui, and Saoula (2017), noted that the substrate bias voltage could helpful in orienting growth and improve the crystallinity of TiO2 thin films. The study also revealed that by increasing the ionization density and the incoming particles energy, the surface smoothness of the thin films could be altered. Similar findings were found in a study by Shi, Shum, Zhou, and Li (2017), whereby with further increasing negative substrate bias, the surface morphology of CeO_{2-x} exhibited a completely different trend of roughening. The author mentioned that there are generally two competing processes exist during the sputtering: etching and deposition of the deposited material. These two opposite effects are both associated with the ion energy. Hence, the coating growth and the surface morphology are directly determined by the energy of depositing ions.

Table 2.1 summarized the various research groups' investigation to study the effect of different parameters on properties of silicon nitride thin film and silver film system.

Table 2.1. Review of silver thin films and silicon nitride thin films.

No.	Type of PVD	Target	Target-substrate distance	Bias voltage	Gas	Sputtering pressure	Deposition power	Substrate temperature	Findings	Reference
1.	DC magnetron sputtering	Ag (99.99%)	-	-	Ar	0.05-2.8 Pa	0.5-5.0 kW	250 ºC	• Thickness = 60 nm- 1µm High film density, compressive stress and lower impurity content at high sputtering power	(Y. S. Jung, 2004)
2.	DC magnetron sputtering	Ag (99.99%)	10, 15, 20 cm	-	Ar (5 sccm)	-	100 mA 1 s	-	• Target-substrate distance affect the deposition rate, shape and distribution of particle's position of Ag • Optimum distance = 20 cm Ag size = 1/(t-s distance*I)	(Asanithi et al., 2012)
3.	RF magnetron sputtering	Ag (99.99%)	-	-	Ar / N_2	2 Pa	10, 20, 30 kW	Room, liquid nitrogen substrate temperature	• Grain size affected by sputtering power and time Microstructure and morphology affected by sputtering gas	(Xiong et al., 2000)
4.	DC magnetron sputtering	Ag (99.99%)	5 cm	-	Ar	0.05-2.8 Pa	0.5-5.0 kW	250 ºC	• Effective ion bombardment induced better adatom mobility Higher sputtering power helpful for higher fraction of (111) grain, higher film density.	(Y. S. Jung, 2004)

5.	DC magnetron sputtering	CrSi	6 cm	0, -100, -200, -300 V	Ar / N_2	0.5 Pa	150 kW	100, 300, 500 ºC	• Thickness is about 2.5-4.0 µm • CrN orientation (111) change to (200) with increasing bias voltage but independent of the substrate temperature. • Microhardness affected by bias voltage through preferred crystal orientation.	(Tan, Zhang, Wu, Fang, & Jiang, 2011)
6.	Magnetron sputtering	CrSiN	5 cm	-	Ar / N_2	1.33 Pa	Cr (175 W) Si (50 W)	373 – 773 K	• Increasing N2 content decreased the Ra • Grain size increase, RMS decrease with temperature increase	(Shah et al., 2011)
7.	Reactive magnetron sputtering (review paper)	Si	-	-	-	-	-	-	• SiN with good adhesion, low level compressive residual stress prepared under: • 600 mPa, substrate temp < 200ºC, negative bias > 100 V	(Hänninen, 2018)
8.	High power impulse magnetron sputtering (HiPMS)	Si (99.99%)	-	-100 V	Ar / N_2	-	1-4 kW	110, 430 ºC	• Smooth, dense, homogenous microstructure was obtained • Thickness = 1.2 ~ 4.4 µm • Si-N bond dominant High power, Si-Si bond formed	(Maria Pettersson et al., 2013)

In this work, the arguments discussed above were considered in selecting the parameters for deposition of silver silicon nitride coating. As the research study is to investigate the influence of bias voltage on the silver silicon nitride depositions, hence the author varied the bias voltage parameter meanwhile the rest of parameters were kept constant.

2.5 Summary

Due to the excellent mechanical and biocompatibility properties, Ti64 alloy was chosen as substrate to be used in this study. Meanwhile, silver and silicon nitride were selected as the coating layer to protect the substrate as well as to enhance the Ti64 bulk properties. Magnetron sputtering technique was selected as the coating technique due to its benefit as per discussed.

CHAPTER 3: MATERIALS AND METHODS

3.1 Introduction

Material used as a substrate in this research study was Ti64 alloy that composed of 6% of Aluminum, 4% of Vanadium, 0.25% of Iron, 0.2% of Oxygen and around 89.55% of Titanium. Target used in this research study were silver and silicon which both have 99.99% of purity. Meanwhile, pure Nitrogen was flowed into the chamber during the co-sputtering process. The overall flow from the sample preparation until characterizations process were illustrated in a flow chart shown in Figure 3.1 In this chapter, the details of each stage will be explained further in this chapter.

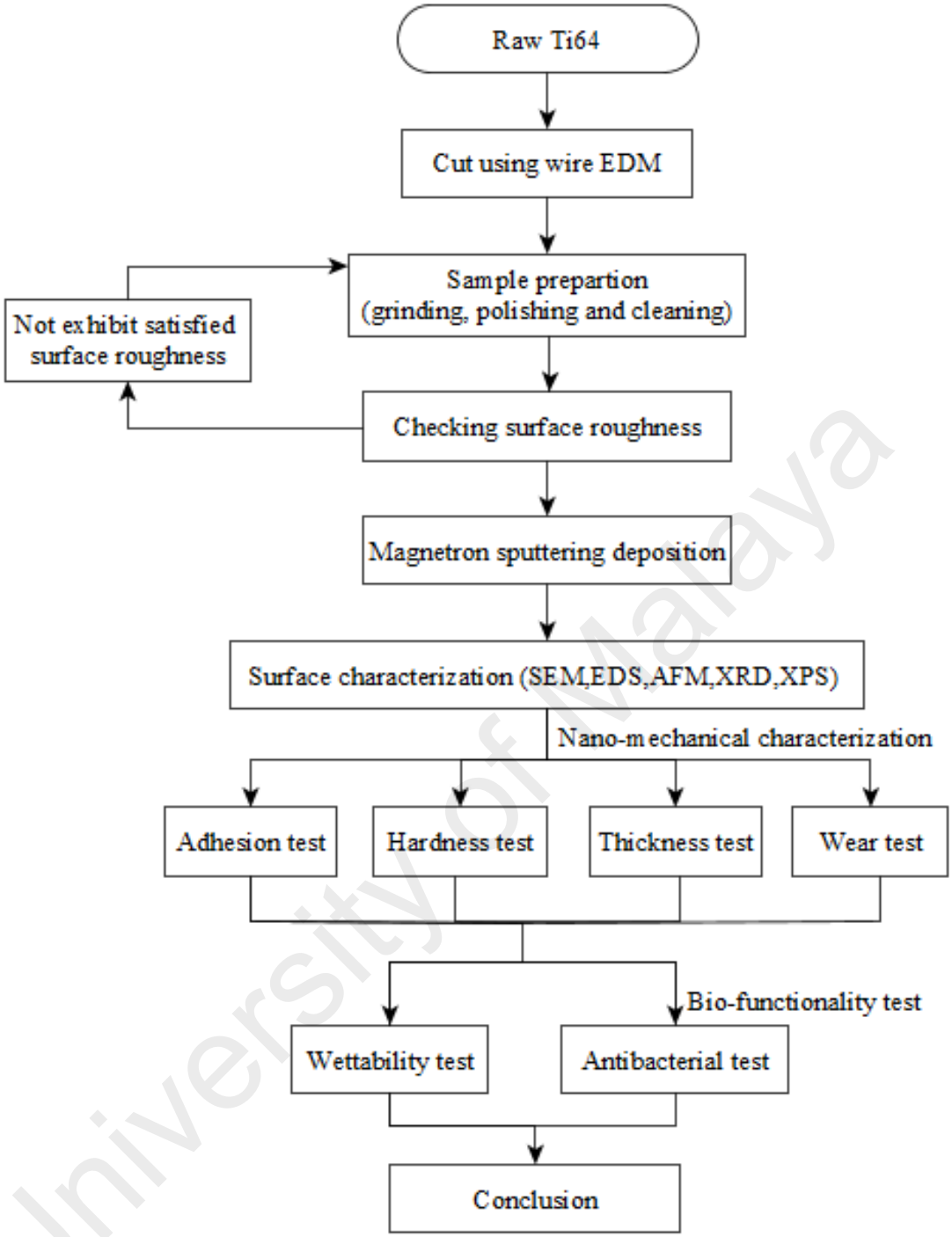

Figure 3.1. Methodology flow chart

3.2 Sample preparation

Grade 5 Ti64 alloy raw material was cut using electrical discharge (EDM) machine into 15 x 15 x 2 mm in size. The working surface was then grounded with SiC abrasive paper starting from 800, 1000, 1500, 2000 and 2500 grit using a Scientific Metapol-2 grinder and polisher equipment. At every change of Silica carbide abrasive paper, the working surface was rotated by 90^0 so that the scratches produced by the subsequent grit paper 'eating up' scratches produced from the previous low Silica carbide grit papers. Next, substrates were polished using polishing cloth aided with the diamond slurry of 6 μm and 3 μm until mirror finished. The surface roughness of the substrate would be around < 1.0 μm measured with Mahr Perthometer. The topography of the substrate surface before deposition plays an important role in film formation. In this study, the substrate roughness is prepared to have an average of < 1.0 μm surface roughness as this value seems to fulfil the condition and potential in producing a durable growing film on substrates as according to the literatures. Before substrates were loaded into deposition chamber, they were ultrasonically cleaned with acetone at temperature 20 °C and 18 kHz frequency for 15 minutes, rinsed with distilled water and subsequently dried using a blow dryer. During the substrate grinding, polishing process and after blow dried, all samples were observed and examined under light optical microscope to ensure that there is no major scratch on the working surface. For thickness measurement purpose, part of the substrate was covered with Kapton tape. The process of grinding, polishing, cleaning and drying prior to deposition process were done in order to remove any oxide layer, moist, dirt and contaminants on substrate's working surface. A good sample preparation can lead to the improvement in terms of quality and adherence of the deposited coating.

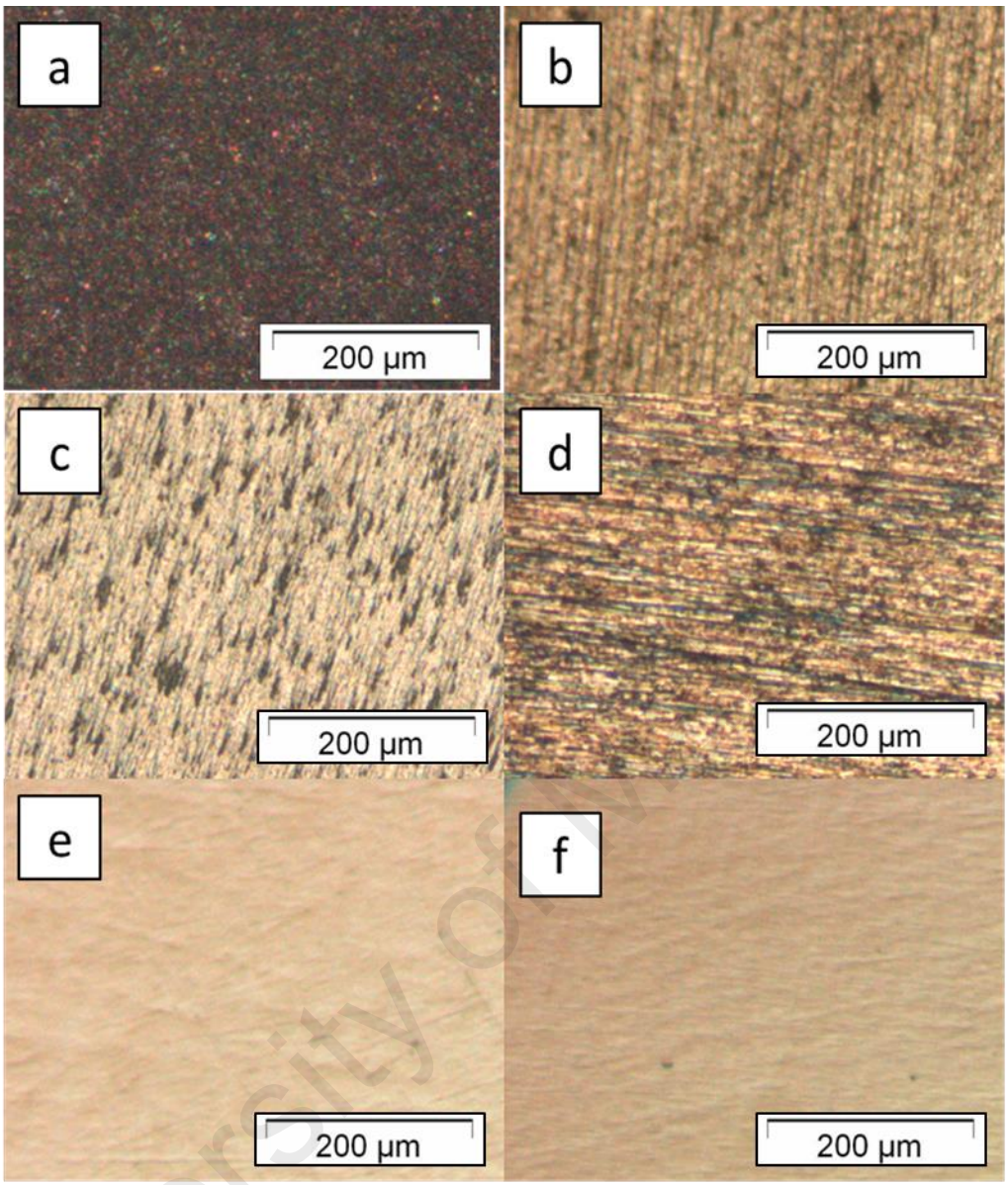

Figure 3.2. Surface view of Ti64 substrate during grinding and polishing process (a) before grinding, (b) 1500, (c) 2000, (d) 2500, (e) polished with 6 µm diamond liquid and (f) polished with 3 µm diamond liquid.

3.3 Deposition setup

Ti64 substrates were deposited with silver target (99.99% purity) connected to DC power supply co-sputtering along with silicon target (99.99% purity) connected to the RF power supply. The deposition process was done using the SG Control Engineering Pte. Ltd machine in Engineering Faculty, University Malaya. The chamber (400 x 500 x 500 mm^3) was manually cleaned using ethanol solution and covered with aluminum foil in

order to minimize any contaminations cause from previous deposition. After that, cleaned working surface substrates were mounted in the middle of the circular substrate holder with a diameter approximately 300 mm. The power applied to Ag and Si target were 20 W and 100 W accordingly. Meanwhile, the distance between substrate-target distance and substrate rotation were all fixed at 15 cm and 30 rpm respectively. Prior pre-sputtering process, the chamber was vacuumed to a base pressure of 2×10^{-5} Torr. Once the desired base pressure was achieved, pure Argon gas (40 sccm) was introduced into the chamber for 20 minutes while shutters still shut both of the targets. The purpose is to remove any oxide layer that present on the target surface. The silver silicon nitride coating was attained by co-sputtering silver and silicon target. At the same time, nitrogen gas was introduced (8 sccm) into the chamber and kept the Argon gas from the pre-sputtering process. The working pressure around 6.3×10^{-3} Torr was maintained throughout the deposition process. In order to study the influence of bias voltage on silver silicon nitride properties, all deposition parameters were kept constant except for the bias voltage. Bias voltage parameter was altered from 0, -75, -150 and -200 V. To avoid unnecessary thermal stress on the samples, all the coated samples were taken out from chamber after being cooled down. The experimental parameters was tabulated in Table 3.1.

Table 3.1. Experimental parameters

Deposition parameter	Unit	Values
Base pressure	Torr	2×10^{-5}
Pre-sputtering	min	20
Ar gas flow	sccm	40
N_2 gas flow	sccm	8
Working pressure	Torr	6.3×10^{-3}
Silicon target power	W	100
Silver target power	W	20
Substrate rotation	rpm	30
Substrate bias voltage	V	0, 75, 150, 200
Deposition time	min	60

3.4 Surface characterization and analysis techniques

By using the PVD method, the substrate's surface was engineered according to the user needs, therefore, it is important to know what is happening on the substrate's surface. In this research study, the morphology, topography, surface binding energy, crystallite size and microstrain of deposit coatings were investigated. Each characterization will be explained in details as below.

3.4.1 Surface morphology

Scanning Electron Microscopy (SEM) with 10.0 kV and 10 000 magnification was used to observe and study the surface and cross section morphology of coatings. The SEM equipment is equipped with Electron Dispersive Spectroscopy (EDS), which is used to obtain the elemental compositions of coatings. Apart from SEM-EDS equipment, optical microscope of OLYMPUS BX61 with 10 magnification was used to observe the surface morphology of the scratch track after the scratch test.

3.4.2 Surface topography

The coatings were further investigated by a non-contact mode tip of atomic force microscope (AFM) of Park NX10 AFM to understand the coatings topography. Meanwhile, XEI software was used to analyse the SPM data. From the AFM equipment, 2D and 3D image of the coating's surface was obtained which revealed surface features which could not be seen from SEM equipment. Besides, the surface roughness information was also extracted from either line view, region view or surface view. Generally, all these three views will give users more or less same surface roughness value.

3.4.3 Crystal structure

Investigation on phase structure, crystallinity, texture coefficient, crystallite size, microstrain as well as residual stress of the coatings were explored by X-ray diffraction (XRD) of Empyrean PANalytical equipment. The equipment was set with voltage and power at 40 kV and 40 mA accordingly. Using XRD thin film run setup, substrate was beamed with Cu-Kα radiation source (λ= 1.54060 Å) at room temperature. The diffractometer rotation range and step size were fixed at $2\theta = 20^0$ - 80^0 and 0.0260 respectively. The principle of XRD can be explained by the Bragg's law concept whereby the beam of x-rays enters a crystal, the diffracted peaks observed carrying two conditions i) the angle of incidence is equal to the angle of diffracted and ii) the difference of path length is equal to the integer number of wavelength.

$$n\lambda = 2dsin\theta \tag{3.1}$$

Where n is the reflection order, λ is x-ray wavelength, d is the full width at half maximum (FWHM) of selected peaks. The visualization of Bragg's law is depicted in Figure 3.3 below. The sample's phase analysis was done by comparing the x-ray pattern with database prepared by an institution such as International Centre for Diffraction Data (ICSD).

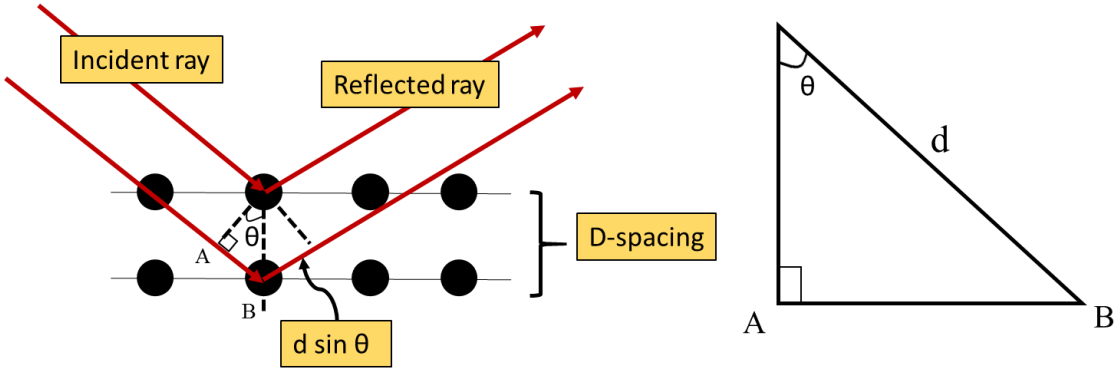

Figure 3.3. Visualization Bragg's law.

Apart from the phase determination, crystallite size and microstrain values can also be obtained from the XRD data along with other analysis method such as Scherer's formula, Williamson and Hall method (W-H) and Warren Averbach analysis (W-A). Scherer formula only gives the lower bound of the crystallite size values and therefore the equation neglects the other important factors such as inhomogeneous strain and instrumental effects broadenings. For W-A analysis, it is reported to have a rigorous and unbiased approach in analyzing the XRD broadened profile, but due to the overlap in the sample's broadening, large error might occur in this approach. Moreover, W-A method usually used together, along with other methods such as Voight function and Stokes deconvolution which make the method quite a complicated analysis (Ghosh, Chattopadhayay, Meikap, & Chatterjee, 2008). As for W-H analysis, it is a simplified integral breadth method and clearly differentiate size and strain induced peak broadening by considering the peak width as a function of 2θ. W-H analysis is considered to be an average method, but still holds an unavoidable position for crystallite size determination (Venkateswarlu, Chandra Bose, & Rameshbabu, 2010). Another method that can be considered is the Approximation Method by Bushroa, Rahbari, Masjuki, and Muhamad (2012). Approximation Method was shown a reliable technique in measuring crystallite size, as crystallite size values obtained using this method has a small deviation compared to the real value measured from the SEM image. In the presented work, the crystallite

size and microstrain values in AgSiN thin films are determine using the Approximation Method. The next subsection 3.4.4 will explain in details the Approximation Method used.

3.4.4 Determining crystallite size, microstrain and residual stress via Approximation Method

In this research study, the uprising method which is Approximation Method by Bushroa et al. (2012) will be utilized to find the crystallite size and microstrain values. From the crystallite size and microstrain values, the residual stress exists in the thin film could be projected. There is a need to understand the changes in crystallite size, microstrain and residual stress under different deposition condition as the information can be used to understand the failure happening in the thin films hence giving idea to researchers in improving the material properties.

The total physical broadening denoted as *(β)* is the sum of the particle size broadening *(m)* and strain broadening *(n)*. Other factors that contributed to the physical broadenings are assumed negligible. Using the Approximation Method, the contribution of size and strain factors can be separated. Denoted that *M(2θ)* and *N(2θ)* represent the profile broadening and strain broadening functions. The correlation between *β, m*, *n, M(2θ)* and *N(2θ)* are described by equations below (Bushroa et al., 2012).

$$\beta = \frac{nm}{\int N(2\theta)M(2\theta).d(2\theta)} \tag{3.2}$$

where,

$$m = \frac{\int M(2\theta).d(2\theta)}{M_{max}} \tag{3.3}$$

and,

$$n = \frac{\int N(2\theta).d(2\theta)}{N_{max}} \tag{3.4}$$

Assumed that the approximated profile for *M(2θ)* and *N(2θ)* are:

$$M(x) = (1 + yx^2)^{-1} \tag{3.5}$$

$$N(x) = (1 + yx^2)^{-2} \tag{3.6}$$

Where y is a constant coefficient. Therefore, the relationship between *β, m* and *n are:*

$$n = 0.5 * \beta \left(1 - \frac{m}{\beta} + \sqrt{1 - \frac{m}{\beta}}\right) \tag{3.7}$$

In the Approximation Method, two peaks (the most far right and far left) were considered. From the XRD diffractogram in Figure 4.4, two peaks identified were $\theta_{111} = 38.1°$ and $\theta_{113} = 77.46°$. These two peaks have respective integral broadening of β_1 and β_2 at (111) and (113) orientation. Considering the particle size broadenings, m_1, m_2 and strain effects broadenings, n_1 and n_2. The derivation is as the following:

$$\beta_1 = \frac{(m_1 + 2n_2)^2}{m_1 + 4n_1} \tag{3.8}$$

$$\beta_2 = \frac{(m_2 + 2n_2)^2}{m_2 + 4n_2} \tag{3.9}$$

New parameter V and W are introduced.

$$V = \frac{m_2}{m_1} = \frac{cos\,\theta_{111}}{cos\,\theta_{113}} \tag{3.10}$$

$$W = \frac{n_2}{n_1} = \frac{tan\,\theta_{111}}{tan\,\theta_{113}} \tag{3.11}$$

Then, (3.12) and (3.13) were derived by solving (3.8) – (3.11)

$$\frac{m_1}{\beta_1} = \frac{1}{2} - 4\frac{n_1}{\beta_1} + \sqrt{1 + 8\left(\frac{n_1}{\beta_1}\right)} \tag{3.12}$$

$$\frac{\beta_2}{\beta_1} = \frac{\{[V(m_1/\beta_1)] + [2(n_1/\beta_1)W]\}^2}{[V(m_1/\beta_1)] + [4(n_1/\beta_1)W]} \quad (3.13)$$

Assume that (n_1/β_1) values were in the range of 0-1 with an increment of 0.1. The (m_1/β_1) values then can be calculated using (3.12) and *(β_1/β_2)* from (3.13). The (m_1/β_1) values were plotted against *(β_1/β_2)* presented in Figure 4.7. Both of these plots were used as reference to find the experimental values of $(m_1/\beta_1)_{exp}$ and $(n_2/\beta_2)_{exp}$. For example, given that the experimental value *(β_1/β_2)$_{exp}$* of θ_{111} 38.1° into the Figure 4.6 graph would lead to the (m_1/β_1) value. Similar way was done to obtain the (n_2/β_2) value. The m_1 and n_2 values were then obtained by multiplying the (m_1/β_1) and (n_2/β_2) with respective broadenings. The crystallite size value and microstrain were calculated using (3.14) and (3.15).

$$D = \frac{k\lambda}{\beta \cos\theta_1} \quad (3.14)$$

The equation (3.14) is known as Scherer's formula where *D* is the estimation of crystallite size, β is the integral breadth of full width at half maximum (FWHM). *K* is a constant (i.e. 0.94), λ is the wavelength of the x-ray radiation (i.e. 0.154 nm) and θ is the Bragg angle θ_{111} *38.1°* reflections. The value of m_1 should be used instead of total physical broadening (β).

$$\varepsilon = \frac{n_2}{4 \tan\theta_2} \quad (3.15)$$

Where ε is microstrain, n_2 is micro-deformation broadening and θ is the Bragg angle of θ_{111} *38.1°* reflections. Both (3.14) and (3.15) can be used if the following condition exists: $0 < (m_1/\beta_1)$ *or* (m_2/β_2) *and* (n_1/β_1) *or* $(n_2/\beta_2) < 1$.

3.4.5 Binding energy (XPS)

The binding energy and elemental compositions of AgSiN thin films were provided by X-ray photoelectron spectroscopy (XPS) (Kratos AXIS Ultra). The coated sample was

mounted inside the chamber and vacuumed at 6.66 x 10^{-8} Pa. The coated sample was then bombarded with Al (mono) Kα X-ray under 12 kV and 10 mA. XPS spectra data were analyzed using PHIMultiPak software. Carbon, C 1s peak of 284.6 eV was used to calibrate the binding energy. The purpose of calibrating was to remove any shifting peaks due to charging during the analysis (Herrera-Gomez et al., 2011). The sample binding energy and elemental compositions were obtained by comparing the energy binding to the NIST X-ray photoelectron spectroscopy database.

3.5 Mechanical characterization techniques

Reliability and durability of the functional coatings can be determined by knowing its mechanical properties. Here, the mechanical properties of coatings such as hardness and elastic modulus were determined using nanoindentation test. The adhesion strength and coating thickness of coatings were determined using a scratch test. Meanwhile, wear properties were obtained using wear test. Details of each characterizations will be further explained in the sections below.

3.5.1 Hardness test

Mechanical properties like hardness and elastic modulus of coatings were explored using T1750 Ubi Hystron-Inc Mechanical Test Instrument equipped with Berkovich diamond indenter. Depth controlled settings was used to avoid any substrate influence in the nanoindentation data. The depth penetration was fixed at 1/10 from the coating thickness. A series of 10 indentations were done and mean values were calculated. Each indentation was separated by about 8 μm to eliminate any influence from neighbor indentations.

3.5.2 Adhesion and thickness properties

The adhesion strength and coating thickness were measured by using the scratch test. The adhesion strength between the thin film and the substrate was obtained in the multi-

pass mode of the progressive scratch test. A diamond tip with 90^0 conical shape and 25 μm radius were straightforwardly pulled along 700 μm on the coated surface with a progressive load start continuously from 0 until 500 mN (1 mN/s). At least three times of scratch tests were done on the sample in order to reduce any error involved meanwhile the light optical microscope was used to confirm the critical load *(Lc)* and critical distance *(Dc)* of the coating.

The result of scratch tests can be affected by intrinsic and extrinsic factors. Intrinsic factor is a factor that related to the scratch test conditions such as scratching speed, indenter shape and loading rate. Meanwhile, extrinsic factor is a factor relevant to the substrate-coating properties such as critical load (Vlcak et al.) value and friction coefficient (COF). Therefore, in order to obtain a reliable and comparable results, the intrinsic factor was kept constant throughout the scratch test study. The scratch test is connected to a monitor where it displayed a real time scratching distance versus the load, scratching distance versus load graph and scratching distance versus the friction graph. The *Lc* and *Dc* can be noted when there is an abrupt change in scratching distance versus depth graph. The *Dc* value is then can be confirmed from the image obtained from the light optical microscope.

In order to determine the coating thickness, part of the substrate's surface was covered with Kapton tape prior the deposition process. After the deposition process was done, the Kapton tape was removed, thus revealed the coated and uncoated regions. The diamond stylus will move across from the coated to uncoated region at minimum load 2 mN. The difference in step height will give the coating thickness value.

3.5.3 Wear test

The coefficient of friction of the thin was investigated using the pin-on-disk tester (DUCOM pin-on-plate reciprocating friction monitor TR-282). A cylindrical pin which

have diameter of 6 mm and 8 mm length was used. Prior test, all pins and samples were cleaned in distilled water and degreased in acetone. In the dry-sliding test, the pin slid against the stationary counterpart plate. A 5 N of normal loads was applied to the disc. An electro-motor was used to generate the reciprocating motion. The coefficient of friction was calculated by divide the frictional force by the normal load.

3.6 Wettability test

The coating surface wettability was measured using a video-based optical contact angle measuring system of OCA 15 EC Data Physics Instruments GmbH, Germany. Wettability test were done by dropping a drop of deionized on the coating surface with liquid volume and dropping velocity were fixed at 10 µl and 2 µl/s accordingly. The contact angle (*θ)* was obtained by calculating the droplet height *(h)* and width *(d)* using the following equation:

$$\theta\ (^{\circ}) = 2\ tan^{-1}(^{2h}/_{d}) \tag{3.16}$$

3.7 Antibacterial test

The antibacterial test on AgSiN coating was done at Microbiology Laboratory, University of Malaya Medical Centre (UMMC). Bacteria that were used in this study are *Escherichia Coli (E. coli) - ATCC 29522* and *Bulkholderia Pseudomallei (B.Pseudomallei) - K96243*. The procedure starts with an overnight culture of bacteria adjusted to the working concentration of 600 nm (10^8 cfu /ml). Next, 100 µl of culture spotted were dropped on the nutrient agar and spread. Then, the plates were air dried for 5 minutes before the nano-coated samples were put on top of it. Upon that, the plates were incubated in an incubator at a temperature of 37^0. After 1 week, once the nano-coated samples were removed from nutrient agar, the inhibition zone was observed and

measured. The complete antibacterial test procedures were summarized and presented in Figure 3.4 below.

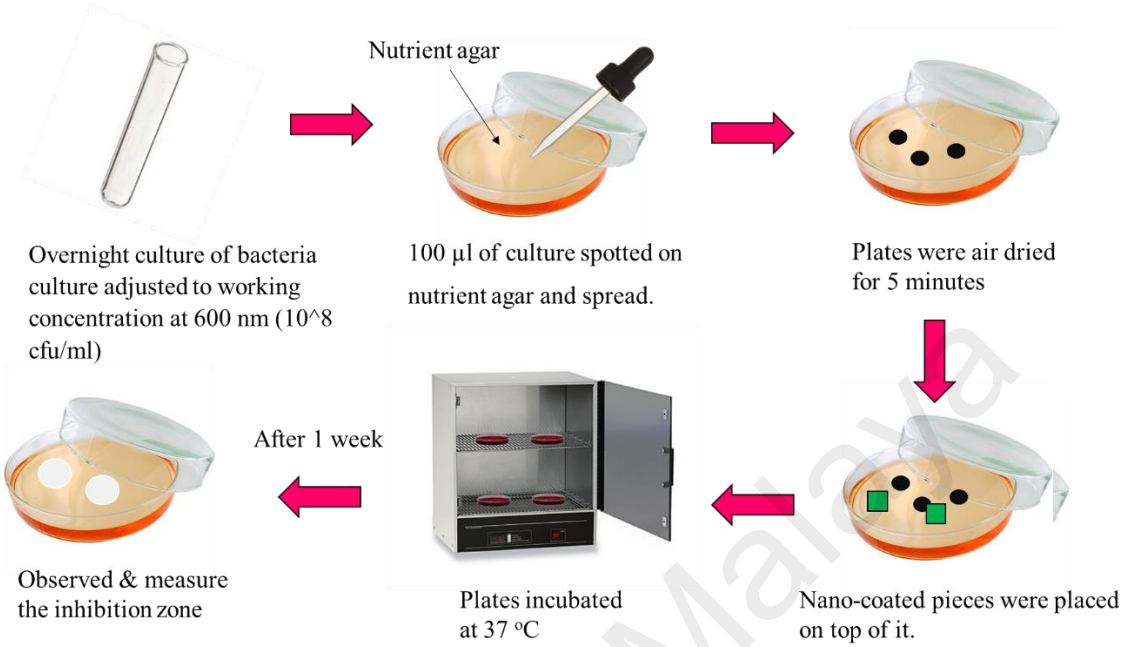

Figure 3.4. AgSiN coating antibacterial test procedure.

3.8 Summary

In this study, the magnetron sputtering method was chosen as the coating technique to deposit silver, silicon and nitrogen on biomaterial Ti64 alloy under a range of bias voltage. This was done in order to investigate the influence of this parameter on the coating properties. Characterizations such as surface, mechanical, wetting and antibacterial were done to study and understand the coating properties.

CHAPTER 4: RESULTS AND DISCUSSION

4.1 Introduction

Once the samples were prepared, depositions were done to study the characteristic of AgSiN thin films under different bias voltages. Upon completing the depositions, the physical-chemical properties such as morphology, compositions, structure and energy binding were studied. Other properties such as hardness, elastic modulus, adhesion strength, wear test, wettability and antibacterial functional ability were also investigated. In this section, the author will discuss the result for morphology, compositions, phase and binding energy in subsection 4.2, determination of crystallite size and microstrain values via the Approximation Method in subsection 4.3, mechanical test results in subsection 4.4 and biological functionality in subsection 4.5. Lastly, sub-section 4.6 will summarized the chapter. The results and discussion in this section will answer the research questions and objectives.

4.2 Morphology, compositions, phase and binding energy analysis

Figure 4.1 illustrated the top view of SEM micrograph of AgSiN thin films deposit under 0, -75, -150 and -200 V bias voltage and the typical cross section of AgSiN thin film. From the micrograph, it can be seen that there were slight changes in microstructures due to the variation of the bias voltage during the deposition process. Films deposited under 0 to -150 V bias voltage exhibit grainy-like structure with no cracks or holes. Meanwhile, at the maximum bias voltage (-200 V), 'dented' features on the films could be observed. This is believed due to re-sputtering effect during the deposition process. Re-sputtering involves the re-emission of material deposited by sputtering during deposition. Similar to the sputtering process, the re-emission is caused by ion bombardment of the deposited material (Vargas et al., 2015). It is generally recognized that the energetic particle bombardment of the growing film induced by the application of substrate bias voltage, promotes the surface adatom mobility and thereby increases the

surface re-sputtering. Generally speaking, when the deposition power is low during the process as the substrate is given a bias voltage, the substrate voltage can act as target and re-sputtering (ion-winning process) is possible which is similar to reactive-ion etching (RIE).

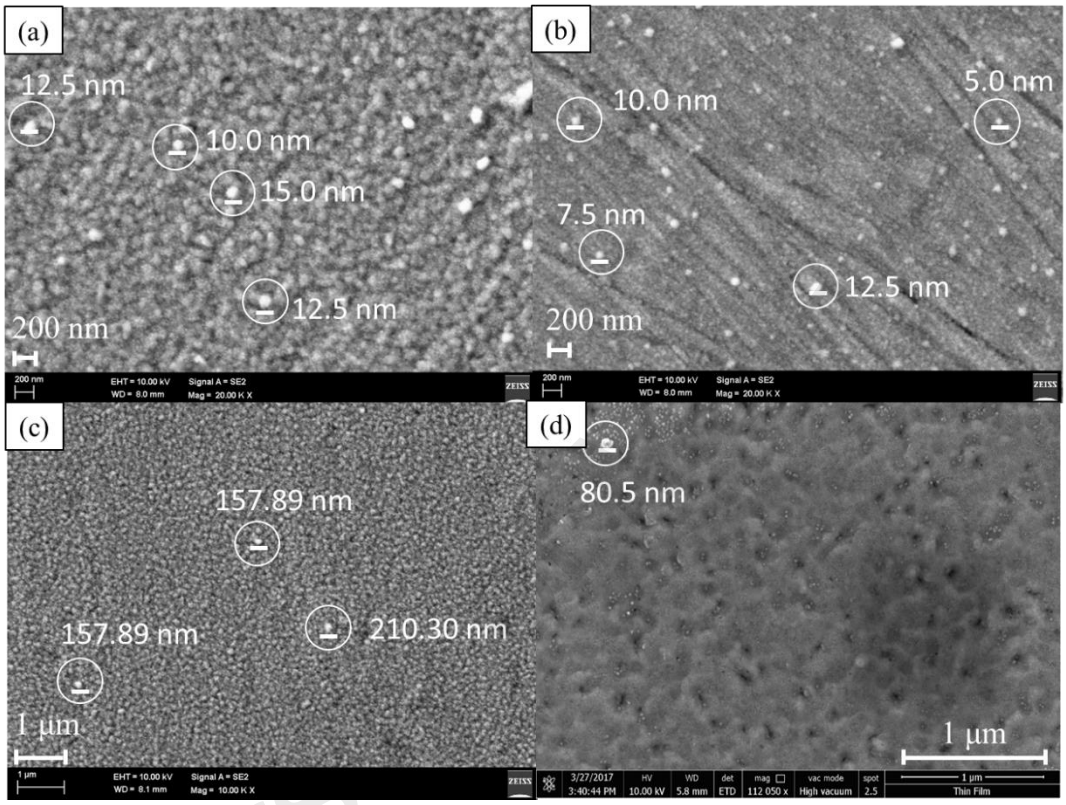

Figure 4.1. SEM micrograph of AgSiN thin film.

The SEM, which equipped with EDS was used to quantify the compositions of the films. Figure 4.2 presented the EDS analysis of all films. From EDS analysis the white nanoparticles observed dispersed on the thin film's surface were confirmed to be sourcing from silver element meanwhile, the background consists of a mixture of silver, silicon and nitrogen elements. The EDS results proved that AgSiN thin films were successfully deposited via the magnetron co-sputtering technique on the Ti64 substrate. From the SEM and EDS result, it can be seen that the nanoparticles which confirmed to be Ag deposit on the Ti64 were dispersed as "clump" and not as a continuous layer. This is important since in order for the film to have antibacterial ability, the film need to have the ability to exposed the active antibacterial ingredients which in the present study is the Ag nanoparticles (Albert et al., 2015; Ali et al., 2014).

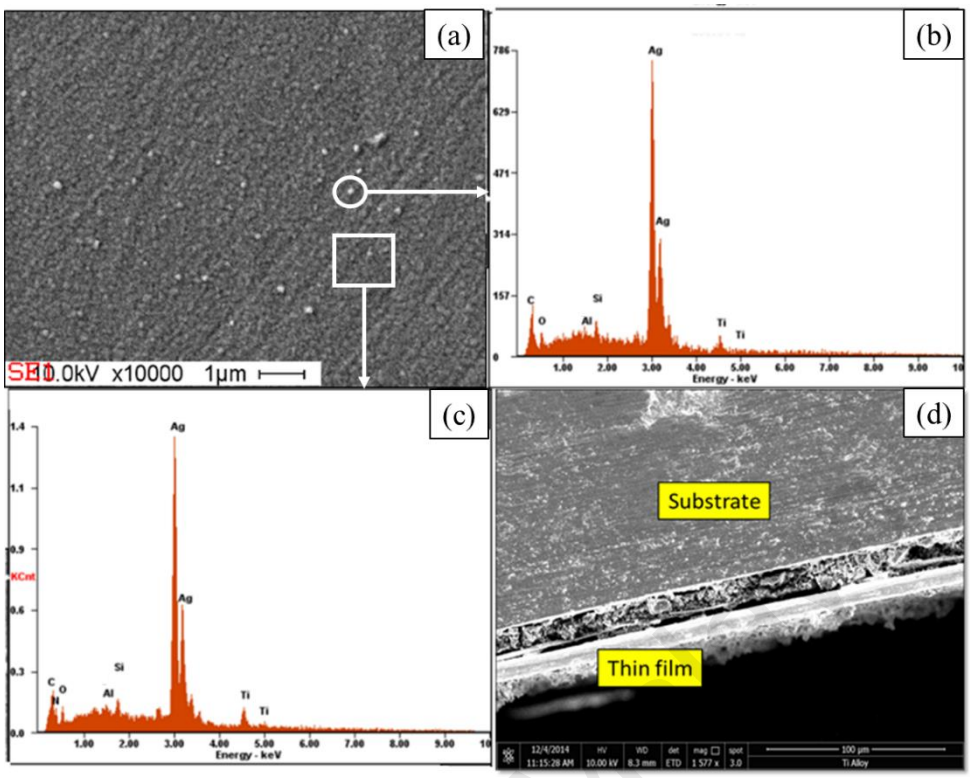

Figure 4.2. (a) SEM micrograph of typical AgSiN thin films, (b) EDS pattern on the selected white spot observed in (a), (c) EDS pattern on the background coating surface as marked with square in (a) and (d) Typical cross section micrograph of AgSiN thin films deposited on Ti alloy.

The influence of substrate bias voltage on the AgSiN film morphology was also confirmed with the AFM (refer Figure 4.3). The surface roughness of the film is increased from 10.5 to 11.9 nm, and it is in consistent with the increment of bias voltage from 0 to -75 V. However, once it reaches -200 V, the roughness is reduced to 5.2 nm. Although this was a small difference in terms of surface roughness measurement in which 6 nm were noted, the roughness may affect other film properties such as wettability (will be explained later). The change in film roughness can be explained by the ion energy or ion flux change during the sputtering process (Q. Ma et al., 2017). The increasing of substrate bias voltages result in an active mobility of the adatoms and thus creates highly nucleation density. Additionally, the highly mobile adatoms may move violently and diffuse into the inter-grain voids under the high-energy ion bombardment. The consequences would be

the films become more compact and denser (Cemin et al., 2017). This is why it is observable that with the increases of negative bias voltage will end up with smoother surface. Therefore, it can be advocated that the bombardment-induced mobility of the depositing adatoms increases with increasing bias voltage leading to a smoother film structure.

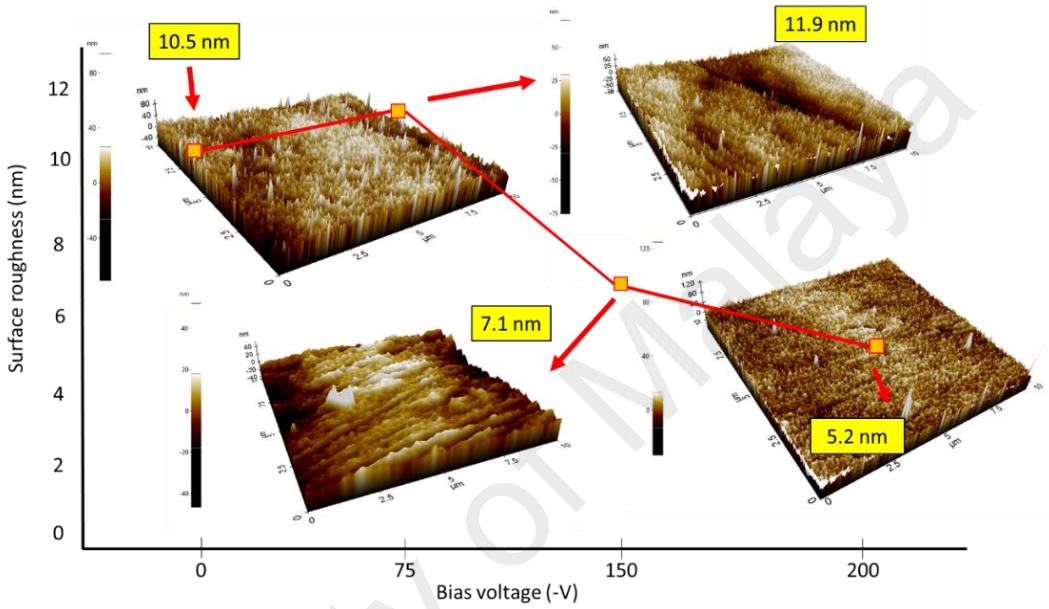

Figure 4.3. AFM morphology of AgSiN thin film deposited at bias voltage ranging from 0 V to -200V.

In order to understand the crystallographic phases, X-ray Diffraction (XRD) measurement was performed and presented in Figure 4.4. It is revealed that the peak positions at 2θ = 38.1° (111), 44.19° (002), 64.48° (022) and 77.46° (113) are belong to the silver phase with face centered cubic (FCC) crystal structure after compared with ICSD No. 98-0040-4387. Besides, hexagonal silicon nitride, Si_3N_4 is also noted but relatively low intensity. The peak position for the Si_3N_4 is observed at position 2θ = 40.35° with ICSD no: 98-003-5660. Aside from silver and Si_3N_4 phases, no other major peaks can be extracted which may suggest that there is no interfacial reaction or bonding between these two phases during the deposition process. Similar results of silver phase

can be observed by other literatures (Ju et al., 2018; Siozios et al., 2014) which deposited silver target via magnetron sputtering technique. The reported crystallographic plane obtained by these literatures were (111), (200), (220) and (311) which were reversed compared to our current AgSiN thin films. Nevertheless, the order of the indices can be neglected since the silver phase is FCC crystal structure whereby the structure basically has the same unit axes of a = b = c and the unit cell angle are $\alpha = \beta = \gamma = 90^{o}$. In other words, the calculated d-spacing for (200) and (002) planes are same given that d-spacing is the distance between planes of atoms which gives rise to the diffraction peaks. It is also noticed that in all scans the phases and peaks of all deposited AgSiN films are more or less consistent. Shift in peaks is a result from the change in the lattice spacing (Obrosov et al., 2017). From the aforementioned discussion, the lattice parameters across the bias voltage are not changes hence the consistency. Furthermore, all peaks are situated in the same position for all coatings and thus no chemical shift could be discerned. This also could indicate the films phase formation stay integrated over all the experimented bias voltage. Aside from silver, hexagonal silicon nitride, N_4Si_3 phase was also noted, but with relatively low intensity. The peak position for the N_4Si_3 was observed at position $2\theta = 40.35°$ with ICSD no: 98-003-5660.

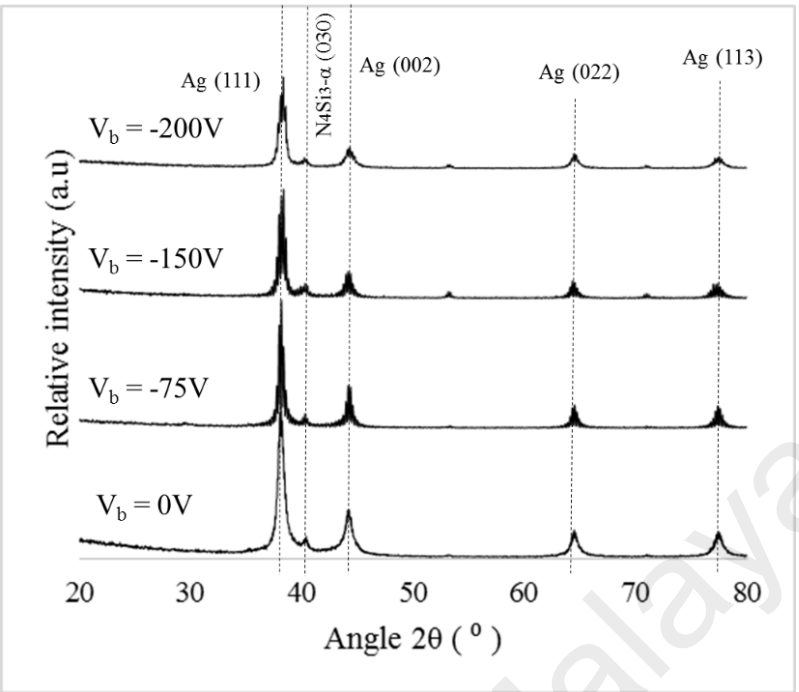

Figure 4.4. XRD pattern of AgSiN thin film

The chemical states on the thin film's surface was investigate using the X-ray photoelectron spectroscopy (XPS). Figure 4.5 presents the XPS wide scan spectra and high resolution of Ag 3d, Si 2p and O 1s for AgSiN coating deposited at a bias voltage of -200 V. The content of Si_3N_4 in AgSiN coating is evaluated from the fit of the Si 2p spectrum. The Ag peaks at 367.7 and 368.4 eV correspond to Ag_2O and Ag respectively. Meanwhile, the Si 2p peaks at 101.8, 103.1 and 103.8 eV are assigned to Si_3N_4, SiO_2 and SiO_2 accordingly. The low nitrogen peak intensity can be due to the small amount of nitrogen gas (8 sccm) used during the deposition. Meanwhile, the incorporation of oxygen in nitride coatings can be correlated with oxidation during the sample handling (Vladescu, Braic, Braic, & Balaceanu, 2013).

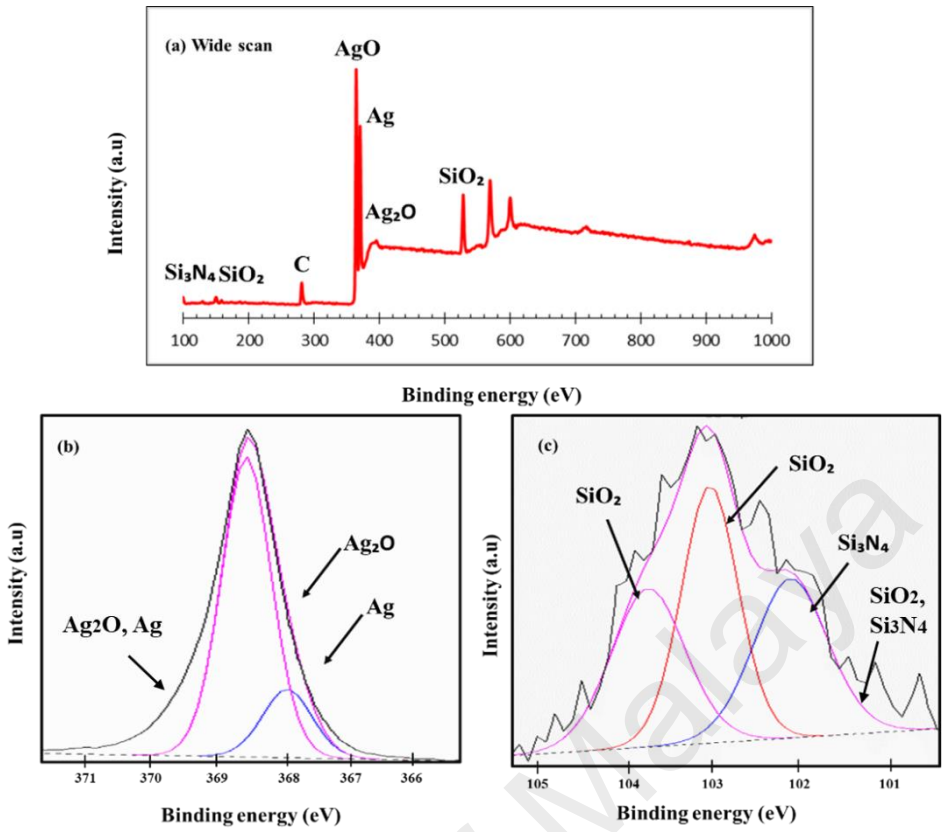

Figure 4.5. XPS spectra for AgSiN thin films deposited at bias voltage of -200V: (a)c wide scan spectra, (b) Ag3d and (c) Si 2p.

Once the surface characterizations of the thin films were studied, the author will present the crystallite size and microstrain determination via the Approximation Method. The microstrain values were then used to project the residual stress. These parameters were important in order to further understand the thin films behavior especially in mechanical properties which will be discussed in sub-section 4.3.

4.3 Crystallite size, microstrain and residual stress via Approximation Method

4.3.1 Crystallite size values determination

As explained in the methodology section, there are several methods that can be used to determine the crystallite size and microstrain values in thin films such as Williamson-Hall (W-H) plot, Warren-Averbach (W-A) and others. In this study, the author opted the Approximation Method to calculate the crystallite size and microstrain values as the

method is convenient, less time-consuming and shown to have a good reliability result. In order to prove the reliability, the author compared the crystallite size and microstrain values in the Approximation Method with the W-H method. W-H method is considered to be an average method but still hold a good reference for the crystallite size determination aside from the TEM micrograph (Khorsand Zak, Abd. Majid, Abrishami, & Yousefi, 2011; Mote, Purushotham, Dole, & Physics, 2012).

For crystallite size values determination, a reference plot was constructed and presented in Figure 4.6. The broadening ratio $(\beta_1/\beta_2)exp$ of the two peaks $\theta_{111} = 38.1°$ and $\theta_{113} = 77.46°$ for thin films prepared under bias voltage 0, -75, -150 and -200 V are calculated. The $(\beta_1/\beta_2)exp$ ratio were 1.33, 1.00, 0.71 and 1.22 accordingly. These $(\beta_1/\beta_2)exp$ were then fed into the graph.

Figure 4.6 which would lead to the m_1/β_1 value. The m_1/β_1 values obtained were 0.62, 1.20, 1.66 and 1.22 respectively. The m_1 value is then obtained by multiplying with the respective broadenings. The crystallite size value is calculated by substituting the m_1 value into the (3.14) equation. The crystallite size value for thin films prepared under respective bias voltage are 30.75, 14.30, 139.41 and 7.38 nm. The summarized values for broadenings and crystallite size of the thin films with respect to bias voltage were tabulated in Table 4.1.

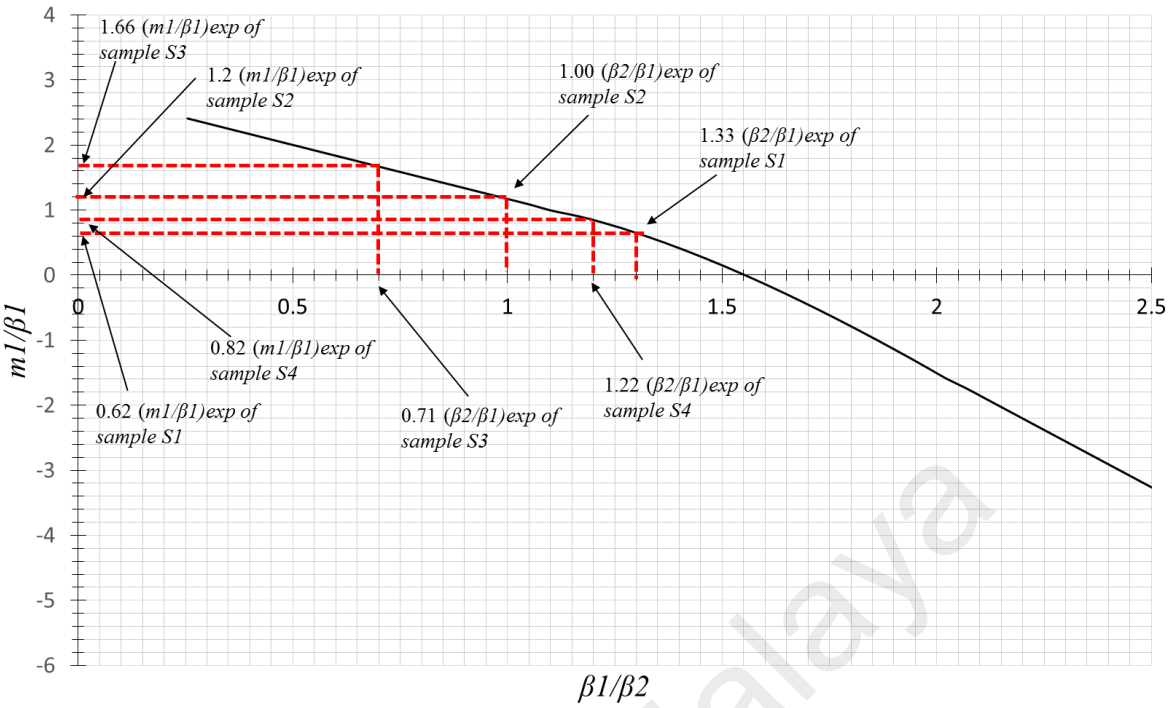

Figure 4.6. m_1/β_1 versus β_1/β_2. A graph representing Approximation Method in determining the crystallite size values.

Table 4.1. Results of Crystallite size calculated using the Approximation Method.

Bias voltage (V)	β_1 at $2\theta = 38.1°$ (radian)	β_2 at $2\theta = 77.46°$ (radian)	$(\beta_2/\beta_1)_{exp}$	$(m_1/\beta_1)_{exp}$	Broadening (m_1)	Crystallite size (nm) using Approximation
0	0.008	0.011	1.33	0.62	5.0×10^{-3}	30.75
-75	0.009	0.009	1.00	1.20	10.7×10^{-3}	14.30
-150	0.012	0.009	0.71	1.66	20.7×10^{-3}	139.41
-200	0.001	0.002	1.22	1.22	1.1×10^{-3}	16.72

4.3.2 Microstrain values determination

Similar method was applied to find the microstrain values. A reference plot was plotted and presented in Figure 4.7. The $(\beta_2/\beta_1)exp$ ratio for thin films prepared under 0, -75, -150 and -200 V were 1.33, 1.00, 0.71 and 0.21 accordingly. These values were fed into the graph which led to the n_2/b_2 values. The n_2/b_2 values obtained were 0.76, -0.20, -1.04 and 0.30 respectively. Then, the n_1 values were obtained by multiplying the n_2/b_2 ratio with the respective broadenings. The microstrain values for thin films prepared under the respective bias voltage were 1.6×10^{-3}, -0.4×10^{-3}, -1.9×10^{-3} and 0.01. The summarized values for broadenings and microstrain of AgSiN thin films with respect to the bias voltage were tabulated in Table 4.2.

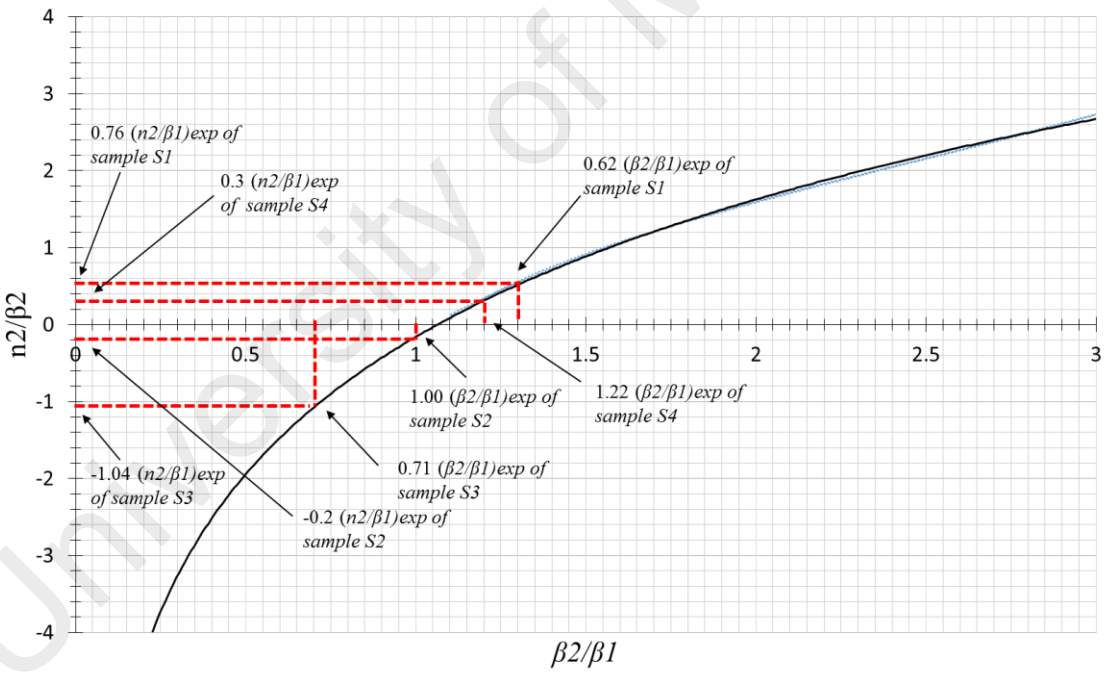

Figure 4.7. n_2/β_2 versus β_2/β_1. A graph representing of Approximation Method in determining microstrain of AgSiN coating.

Table 4.2. Results of microstrain (ε) calculated using the Approximation Method.

Bias voltage (V)	β_1 at 2θ = 38.1° (radian)	β_2 at 2θ = 77.46° (radian)	$(\beta_2/\beta_1)_{exp}$	$(n_2/\beta_2)_{exp}$	Broadening (n_2)	Microstrain (ε)
0	0.008	0.011	1.33	0.76	8.14 x 10^{-3}	1.6 x 10^{-3}
-75	0.009	0.009	1.00	-0.20	-1.79 x 10^{-3}	-0.4 x 10^{-3}
-150	0.012	0.009	0.71	-1.04	-9.28 x 10^{-3}	-1.9 x 10^{-3}
-200	0.001	0.002	1.22	0.30	0.49 x 10^{-3}	0.01

4.3.3 Williamson-Hall (W-H) plot

W-H method is a simplified integral breadth method differentiates size and strain induced peak broadening clearly by considering the peak width as function of *2θ*. In W-H plot method, the B_{hkl} *Cos θ* was plotted against *Sin θ*. From the linear fit line obtained in Figure 4.8, the estimation value of crystallite size and microstrain can be calculated by comparing with the Williamson-Hall plot equation:

$$B\ cos\,\theta = \frac{k\,\lambda}{L} + C\ sin\,\theta \qquad (4.1)$$

The y-intercept give crystallite size the estimation value meanwhile the slope of the graph represents the thin films lattice strain. The presence of tensile stress was indicated by the positive slope meanwhile the presence of compressive residual stress was indicated by the negative slope. Comparing with the W-H equation, the estimated crystallite size values for thin films prepared under 0, -75, -150 and -200 V are 24.06, 17.90, 110.0 and

13.08 nm respectively. For microstrain, the values were obtained for the respective bias voltage are 4.6 x 10^{-3}, -7.71 x 10^{-3}, -0.01 x 10^{-3} and 4.99 x 10^{-4} accordingly.

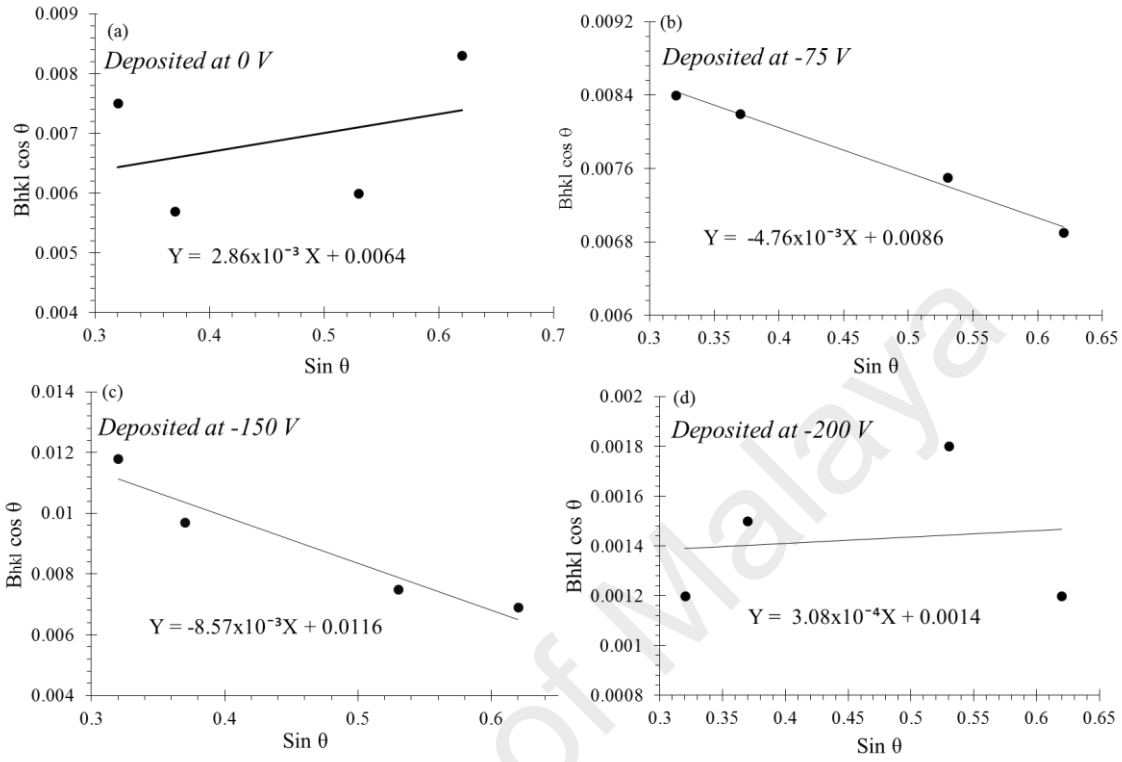

Figure 4.8. Crystallite size and microstrain determination using W-H approach by plotting B_{hkl} *cos* θ vs *Sin* θ of AgSiN coating respective to bias voltage.

Table 4.3. Crystallite size and microstrain values using different methods namely Approximation method and W-H method.

Items	Bias voltage			
	0	-75	-150	-200
Crystallite size $_{Approx.}$ (nm)	30.75	14.30	139.41	16.72
Crystallite size $_{W\text{-}H.}$ (nm)	24.06	17.90	110.0	13.08
Microstrain $_{Approx.}$, ε (no unit)	1.6 x 10^{-3}	-0.4 x 10^{-3}	-1.9 x 10^{-3}	0.1 x 10^{-3}

Microstrain $_{W\text{-}H.}$, ε (no unit)	4.6 x 10^{-3}	-7.71 x 10^{-3}	-0.01 x 10^{-3}	4.99 x 10^{-4}
Stress calculated using n_2 (GPa)	0.18	-0.06	-0.39	0.29

4.4 Mechanical properties (hardness, elastic modulus, adherence and wear test)

Table 4.4 summarized the hardness and elastic modulus of AgSiN thin film obtained from the constant depth mode of nanoindentation tests. According to the results, the hardness values are increased from 2.30 to 5.55 GPa when the bias voltage is increased from 0 to -150 V. The hardness values is then declined to 3.78 GPa when the bias voltage is further increased to -200 V. Similar trend can be observed in elastic modulus whereby the elastic modulus values increase from 113.3 to 211.0 GPa from 0 to -150 V and then decreased to 153.0 GPa at the bias voltage of -200 V. It can be noted that the highest hardness (5.55 GPa) and elastic modulus (211.0 GPa) was observed for film prepared under -150 V. It is highlighted that the hardness and elastic modulus were significantly improved by 50% compared with Ti64 substrate. Given that the hardness and elastic modulus of Ti64 are 2.75 and 113.8 GPa respectively.

This hardening phenomenon observed in AgSiN film could be attributed by several reasons, which are crystallite size and residual stress. Utilizing the Approximation Method (Bushroa et al., 2012) the crystallite size of the thin film were obtained. The calculated crystallite size for AgSiN thin film for 0, -75, -150 and -200 V bias voltage were 30.75, 14.30, 139.41 and 16.72 nm, respectively. As accordance to the inverse Hall-Petch strengthening, the hardness decreases with the decreasing of grain size (Carlton & Ferreira, 2007). This effect implies that nanocrystalline materials get softer as crystallite size is reduced below a critical value. Another factor influencing hardness is residual stress. It is shown that hardness decreases with tensile stress, but increases with compressive stress. The hardening effect could also attribute to the high concentration of

defects due to ion bombardment effect that is not only responsible for the high compressive stress, but also acts as an obstacle for dislocations movement and thus improves hardness (Das, Anwar, Bajpai, & Anwar, 2016). Such residual stress hardening effect was confirmed by previous studies in sputtered TiAlN (Cheng, Han, Liang, Wu, & Zheng, 2013) and TiN/Ni nanocomposite (W. Li et al., 2017) thin films.

Table 4.4. AgSiN coating characteristic (hardness, elastic modulus, adhesion, thickness and coefficient of friction)

Items	Bias voltage			
	0	-75	-150	-200
Hardness, *H* (GPa)	2.30	3.88	5.55	3.78
Elastic Modulus, *E* (GPa)	113.3	162.3	211.0	153.0
Critical distance, *Dc* (µm)	518.77	577.62	359.60	471.09
Critical load, *Lc* (mN)	460	596	476	360
Coating thickness, *t* (nm)	180.0	211.32	100.58	183.20
Coefficient of friction, *COF* (no unit)	0.15	0.04	0.28	0.11

The thin films adhesion strength was studied using the progressive load of scratch test. In scratch test, amount of load where the thin films fail is known as critical load denoted as *Lc*. *Lc* is a point where the thin film delaminates totally from the substrate. Therefore, *Lc* is used as a scale to determine the reliability and durability of the deposited thin films (Bull & Berasetegui, 2006; Volinsky, Moody, & Gerberich, 2002). Figure 4.9 and Figure

4.10 illustrated the scratch track image, depth and friction graph against scratch distance for the respective bias voltage. Meanwhile, Table 4.4 summarized the critical load and critical distance obtained from the scratch tests. From the results, the critical load for AgSiN films prepared under 0, -75, -150 and -200 V were 460, 596, 476 and 360 mN respectively. Meanwhile the critical distance (Dc) were 518.77, 577.62, 359.60 and 471.09 µm, accordingly.

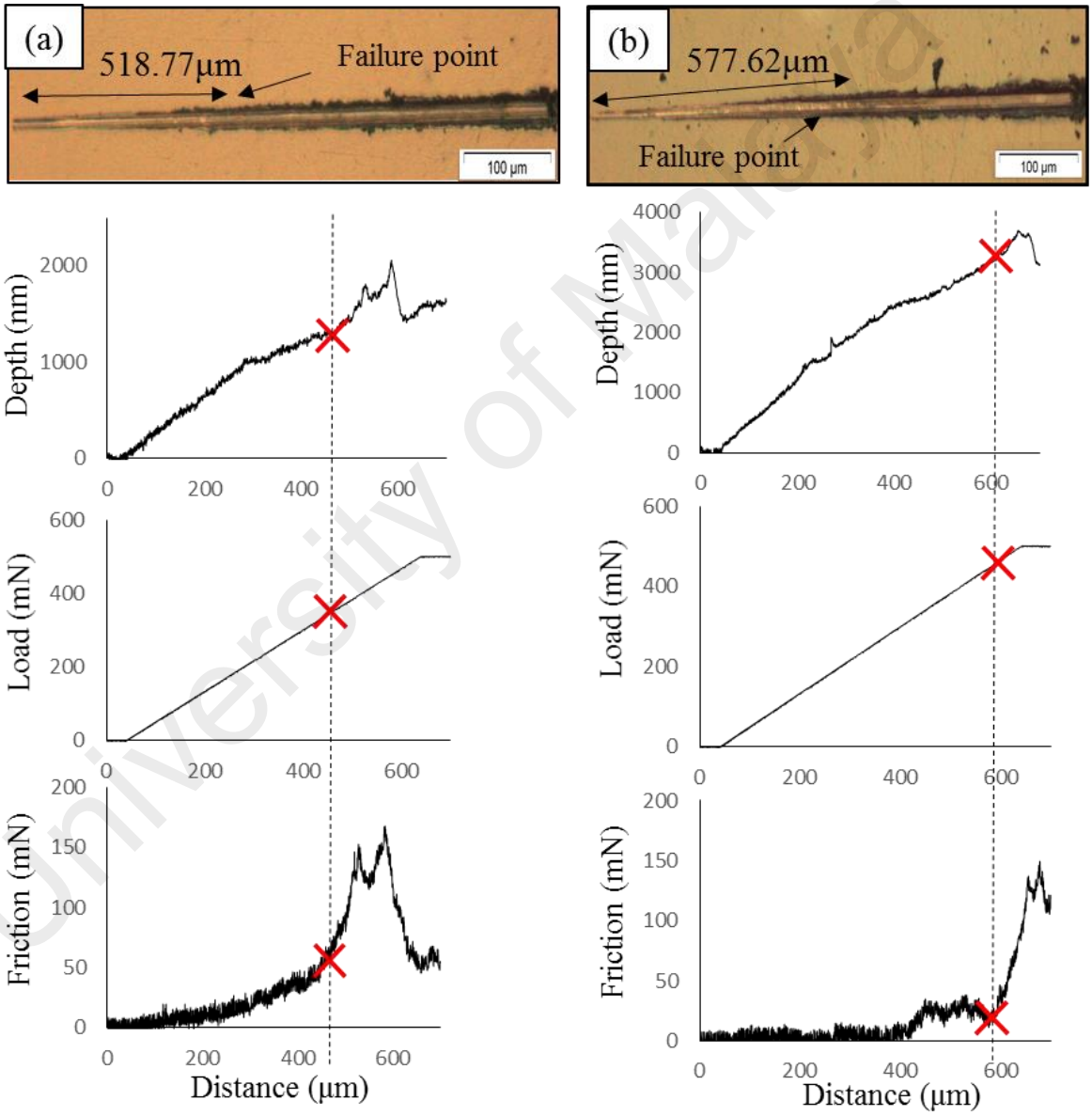

Figure 4.9 .Optical micrograph of scratch track, depth profiles, load and friction graph coating samples prepared at (a) 0V and (b) -75V.

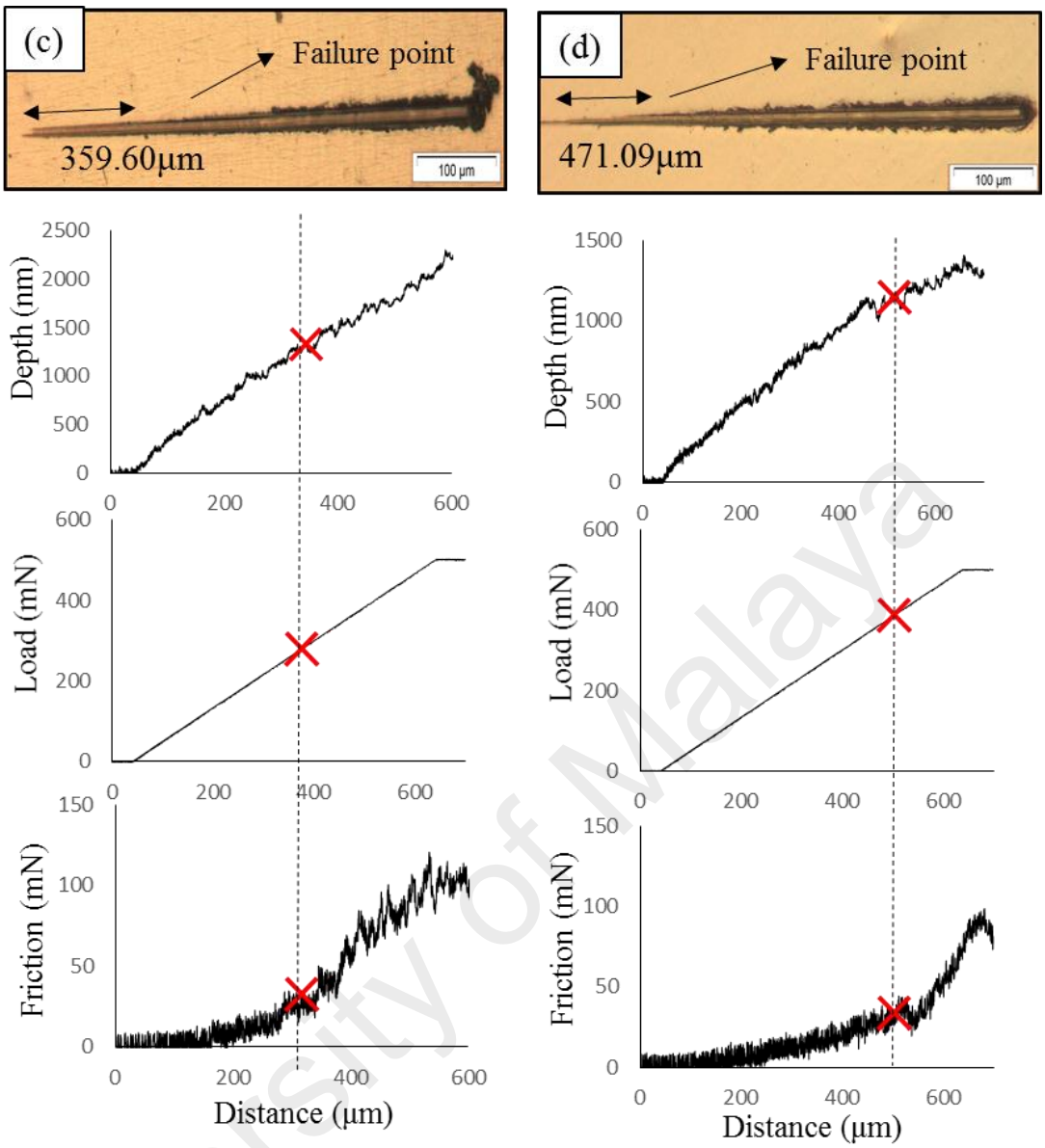

Figure 4.10. Optical micrograph of scratch track, depth profiles, load and friction graph coating samples prepared at (c) -150V and (d) -200V.

All the observed *Lc* was in a good agreement with the calculated residual stresses. Film deposited under -75 V which possessed the highest *Lc* (highest adhesion strength) had the lowest compressive residual stress (-0.06 GPa) as well as the thickest compared to the other specimens. In thicker films, stress that transferred from the surface between the film and the substrate is less. Higher compressive stress is present in thinner films and decreases with the film thickness increment. This can be observed for films prepared under -150 V which has the thinnest thickness (100.58 nm) and highest compressive

residual stress (-0.39 GPa). Generally, under -75 bias voltage, the thickness that allows low compressive residual stress is around 200 nm. Similar behavior could be seen in research study by (J. Liu et al., 2016).

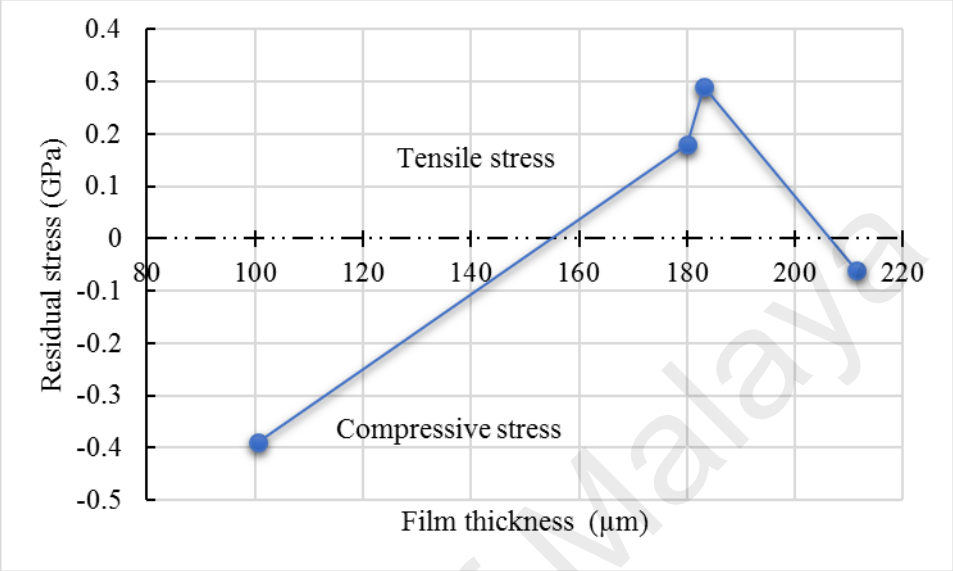

Figure 4.11. Residual stress as function of AgSiN film thickness

Table 4.4 shows the friction coefficient of uncoated Ti64 substrate and AgSiN thin film under different bias voltages. The friction coefficient of Ti64 is 0.18. Meanwhile, the friction coefficient of AgSiN thin film under 0, -75, -150 and -200 V were 0.15, 0.04, 0.28 and 0.11 respectively. The AgSiN thin film friction coefficient improved by 77.77% for sample prepared under -75 V bias voltage. This signifying that the AgSiN coated onto Ti64 substrate had higher wear resistance than the uncoated Ti64. Thus, it can be suggested that high hardness and low coefficient of friction of AgSiN thin film noticeably improved the wear resistance of Ti64 resulted that can be considered in practical applications.

4.5 Biological functionality (wettability and antibacterial test)

4.5.1 Wettability test

The hydrophobic or hydrophilic surface can be signified by the contact angle values from the wettability test. A contact angle value lower than 90˚ indicating hydrophilic

surface properties. Meanwhile, contact angle value more than 90˚ associates with the hydrophobic surface properties. Depending on the targeted applications, hydrophobic or hydrophilic surfaces are selected. Hydrophilicity is preferred when strong interaction with aqueous media is necessary, such as in antibacterial property (Kuroiwa et al., 2018). Moreover, lower contact angle also has been studied to reduce the biological friction, therefore an advantage for bioactive materials. Besides, wettability also appropriate for cell attachment, spreading and proliferation compared to the hydrophobic surface (Ng et al., 2017). Figure 4.12 illustrated the variation of deionized water contact angle on AgSiN thin film under different bias voltage as well as on Ti64 substrate, which is used as reference (control). The contact angle observed are were 86.8˚, 70.9˚, 89.4˚, 82.3˚ and 79.6 ˚ for bias voltage 0, -75, -150, -200 V and Ti64 substrate accordingly. All films exhibit hydrophilic properties in which contact angle was lower than 90˚. The relevance of contact angle with physical properties, particularly with surface roughness was examined. Looking at the surface roughness and contact angle (Table 4.4 and Figure 4.12), there is a minimum in the contact angle such that the angle is larger in the small roughness, reduced for intermediate roughness and then increased with the roughness. Such observations has been studied and it has been found that the role of the surface roughness with wettability is opposite. By increasing the roughness of a chemically hydrophobic surface will enhance its hydrophobicity. Meanwhile by increasing the roughness of a hydrophilic surface, this will further its hydrophilicity. Thus, from these observations, it can be suggested that the surface modifications on Ti64 substrate by AgSiN PVD coating can alter the topography, roughness and wettability.

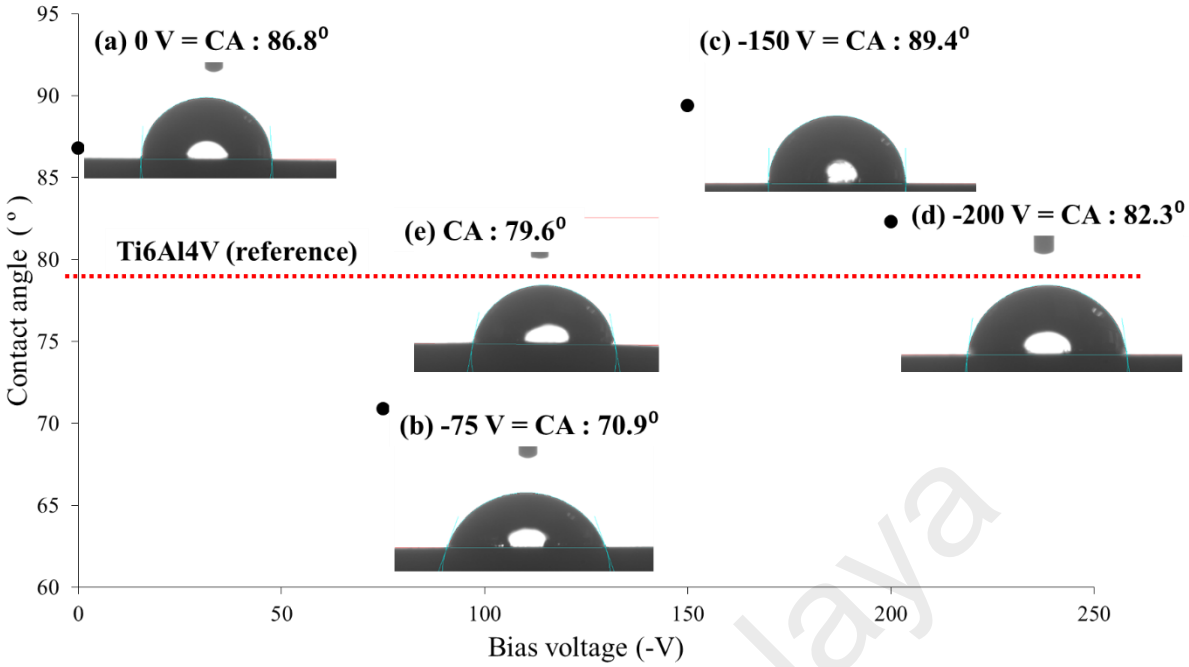

Figure 4.12. Variation of deionized water contact angle on AgSiN coating deposited under (a) 0 V, (b) -75 V, (c) -150 V, (d) -200 V and (e) on Ti64 substrate.

In the next sub-section 4.5.2, the antibacterial ability of AgSiN thin film will be tested through the antibacterial test.

4.5.2 Antibacterial test

The antibacterial ability of the AgSiN film was tested via the antibacterial test. Kirby-Bauer method was opted in this test whereby the antibacterial activity of the films was observed from the inhibition zone after the films were incubated on an agar plate where bacteria have been placed. In this study, the antibacterial ability of the film was tested on two bacteria namely *Bulkholderia pseudomallei (B. Pseudomallei)* and *Escherichia coli (E. coli)*. Since in the antibacterial tests, the thin films will be exposed in harsh environment, the thin films needs to adhere well to the substrate so that it will not peel off during the test. Therefore, for the antibacterial tests, thin films deposited under -75 V was chosen as these sample has the highest adhesion strength (596 mN) in the scratch adhesion test discussed earlier.

Figure 4.13 and Table 4.5 presented and summarized the bacteria inhibition when *B.Pseudomallei* and *E.coli* were exposed to the routine antibiotics and when it was exposed to the AgSiN thin films. The inhibition zone were observed 7 and 10 mm for *B.Pseudomallei* and *E.coli* culture, respectively. As comparison purpose, the bacteria strain was also exposed to the routine antibiotics namely *Ceftazidime (CAZ), Doxycycline (DOX)* and *Tigecycline (TGC).* The average inhibition zone observed when the *B. Pseudomallei* was exposed to the routine antibiotics were 30 *(CAZ)*, 23 *(DOX)* and 13 mm *(TGC).* Meanwhile, the average inhibition zone *E. coli* was exposed to routine antibiotics were 32 *(CAZ)*, 26 *(DOX)* and 15 mm *(TGC)*. It could be observed that the inhibition zone of the bacteria strain on the routine antibiotics were larger when the bacteria are being exposed to the AgSiN thin film. The inhibition zone area of the routine antibiotics on the disk were at least same, doubled or tripled compared to the inhibition zone area of the AgSiN thin films. According to the results, although the antibacterial activity of the AgSiN thin films is not as strong as the routine antibiotics, the AgSiN thin films showed promising potential to be used as biofilms in medical applications.

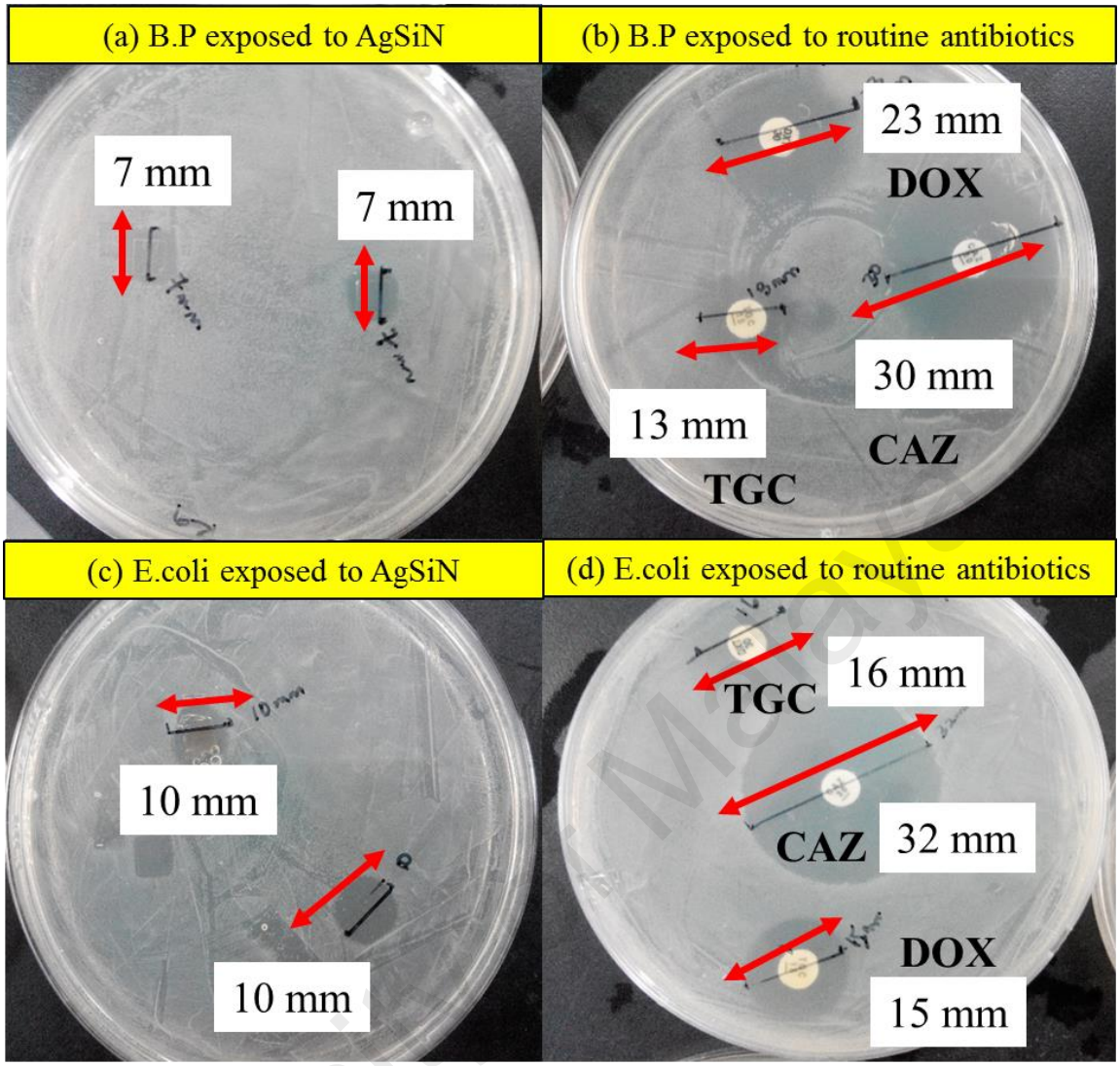

Figure 4.13. Digital photographs show the inhibition zone areas of AgSiN coating on *Escherichia coli* (ATCC 29522), (b) *Bulkholderia pseudomallei* K96243 (reference strain) on AgSiN coated sample. Figure (c) and (d) showed the inhibition zone areas when exposed to routine antibiotics.

Table 4.5 Average inhibition zone of the bacteria strain when exposed to the AgSiN thin films and to the routine antibiotics**.**

Bacteria Strain	Average inhibition zone (mm)			
	Exposed to AgSiN thin film	Exposed to routine antibiotics		
		CAZ	*DOX*	*TGC*
Bulkholderia pseudomallei (B.Pseudomallei)	7	30	23	13
Escherichia coli (E. coli)	10	32	26	15

The theories behind this antibacterial effect can be related to the interaction of Ag+ ions exist on coatings with the agar solution containing bacteria. It is widely known that silver compound and silver ions are toxic to most bacteria. The action of silver on bacteria is not fully known and exactly explained. However, the mechanism of silver compound and silver ions on bacteria can be hypothesized through several sequences. Silver ions have the ability to bind to cell wall of the bacteria, make it more permeable, losing its integrity and thus allows more silver ions to enter the cell. When the silver ions attached to the Sulphur and Phosphorus of the nucleus, they disrupt the function of the cell, destroy DNA which led to DNA replication problem. At the same time, generation of highly toxic reactive oxygen species (ROS) by the cell possibly due to the inhibition of respiratory enzyme are extremely toxic to the cell. All these sequences will eventually lead to cell death (Prabhu & Poulose, 2012).

Since Kirby and co-workers demonstrated that excellent bacterial effects by the reactive metal oxide nanoparticles, it is of great interest to investigate the use of other inorganic nanoparticles such as AgSiN thin film as antibacterial materials. From this study, although the inhibition area of the AgSiN thin film was not par to the routine antibiotics but still the AgSiN thin film exhibit the antibacterial promising candidate.

4.6 Summary

The purpose of this chapter was to present and discuss results obtained from the characterizations including surface, mechanical and antibacterial tests. Finally, functional ability of the thin films was tested through the wettability and antibacterial tests. From the experiments and characterizations, -75 V was found to be the best bias voltage parameter for AgSiN thin film depositions due to its good hardness and elastic modulus, best adhesion strength and wettability. The thin film was also proved to exhibit antibacterial properties.

CHAPTER 5: CONCLUSIONS AND FUTURE WORK

5.1 Conclusions

From the research study, AgSiN thin films were successfully fabricated whereby all the thin films showed homogeneous with uniform and grainy like structure coating. It seems that bias voltage parameter does not give any significant changes on the morphology, topography and phase intensity of the thin films. Meanwhile, tiny dented structure observed probably due to the re-sputtering effect under high negative bias voltage.

Through the Approximation method, the crystallite size and microstrain values were obtained. Using the microstrain values, the residual stress values under varied bias voltage were projected.

From the mechanical, wettability and antibacterial tests, 50 % improvement in hardness (5.55 GPa) and elastic modulus (211.0 GPa) for AgSiN thin films under -150 V. The highest adhesion strength was obtained of AgSiN thin films was obtained under -75 V with Lv = 596 mN and Dc = 577.62 µm. Wettability test showed that all films exhibit hydrophilic properties with lowest wetting angle was 70.9˚ obtained film prepared under -75 V. Besides, AgSiN thin films proved to exhibit antibacterial properties on *E.Coli* and *B.Pseudomallei* with inhibition zone area of 7 and 10 mm respectively.

5.2 Suggestions for future research

First, future research could be used any existing optimization method available such as Orthogonal Array, Taguchi Method or Algorithm Method to find the optimize parameter for the deposition process of AgSiN thin film on the Ti64 substrate. This is because this study provides an investigation one parameter which is the bias voltage on the properties of AgSiN thin films. Second, post thermal treatment process could be done on the as-deposited thin film which could possibly improve the thin film properties. Last but not least, antibacterial test on other types of bacteria could be done in order to study the antibacterial ability of the thin films.

REFERENCES

Albert, E., Albouy, P. A., Ayral, A., Basa, P., Csík, G., Nagy, N., . . . Hórvölgyi, Z. (2015). Antibacterial properties of Ag–TiO2 composite sol–gel coatings. *RSC Advances, 5*(73), 59070-59081. doi: 10.1039/C5RA05990A

Ali, Z. A., Ismail, W. A., Le, C.-F., Jindal, H. M., Yahya, R., Devi Sekaran, S., & Puteh, R. (2014). Antibacterial Coating for Elimination of Pseudomonas aeruginosa and Escherichia coli. *Journal of Nanomaterials, 2014*, 6. doi: 10.1155/2014/523530

Anderson, J. M. (2011). *Biocompatibility and the Relationship to Standards: Meaning and Scope of Biomaterials Testing A2.* Oxford: Elsevier.

Asanithi, P., Chaiyakun, S., & Limsuwan, P. (2012). Growth of Silver Nanoparticles by DC Magnetron Sputtering. *Journal of Nanomaterials, 2012*, 8. doi: 10.1155/2012/963609

Bait, L., Azzouz, L., Madaoui, N., & Saoula, N. (2017). Influence of substrate bias voltage on the properties of TiO2 deposited by radio-frequency magnetron sputtering on 304L for biomaterials applications. *Applied surface science, 395*, 72-77. https://doi.org/10.1016/j.apsusc.2016.07.101

Barillo, D. J., & Marx, D. E. (2014). Silver in medicine: A brief history BC 335 to present. *Burns, 40, Supplement 1*, 3-8. http://dx.doi.org/10.1016/j.burns.2014.09.009

Brandes, E., Brook, G., & Paufler, P. (1993). *Smithells Metals Reference Book.* . Butterworth-Heinemann: Wiley.

Bull, S. J., & Berasetegui, E. G. (2006). An overview of the potential of quantitative coating adhesion measurement by scratch testing. *Tribology International, 39*(2), 99-114. https://doi.org/10.1016/j.triboint.2005.04.013

Bushroa, A., Rahbari, R., Masjuki, H., & Muhamad, M. (2012). Approximation of crystallite size and microstrain via XRD line broadening analysis in TiSiN thin films. *Vacuum, 86*(8), 1107-1112. https://doi.org/10.1016/j.vacuum.2011.10.011

Carlton, C. E., & Ferreira, P. J. (2007). What is behind the inverse Hall–Petch effect in nanocrystalline materials? *Acta Materialia, 55*(11), 3749-3756. https://doi.org/10.1016/j.actamat.2007.02.021

Catalani, S., Stea, S., Beraudi, A., Gilberti, M. E., Bordini, B., Toni, A., & Apostoli, P. (2013). Vanadium release in whole blood, serum and urine of patients implanted with a titanium alloy hip prosthesis. *Clinical Toxicology, 51*(7), 550-556. doi: 10.3109/15563650.2013.818682

Cemin, F., Abadias, G., Minea, T., Furgeaud, C., Brisset, F., Solas, D., & Lundin, D. (2017). Benefits of energetic ion bombardment for tailoring stress and microstructural evolution during growth of Cu thin films. *Acta Materialia, 141*, 120-130. https://doi.org/10.1016/j.actamat.2017.09.007

Cheng, G.-a., Han, D.-y., Liang, C.-l., Wu, X.-l., & Zheng, R.-t. (2013). Influence of residual stress on mechanical properties of TiAlN thin films. *Surface and Coatings Technology, 228*, 328-330. https://doi.org/10.1016/j.surfcoat.2012.05.108

Ciston, S., Lueptow, R. M., & Gray, K. A. (2008). Bacterial attachment on reactive ceramic ultrafiltration membranes. *Journal of Membrane Science, 320*(1), 101-107. https://doi.org/10.1016/j.memsci.2008.03.065

Dakal, T. C., Kumar, A., Majumdar, R. S., & Yadav, V. (2016). Mechanistic Basis of Antimicrobial Actions of Silver Nanoparticles. *Frontiers in Microbiology, 7*, 1831. doi: 10.3389/fmicb.2016.01831

Das, P., Anwar, S., Bajpai, S., & Anwar, S. (2016). Structural and mechanical evolution of TiAlSiN nanocomposite coating under influence of Si3N4 power. *Surface and Coatings Technology, 307*, 676-682. https://doi.org/10.1016/j.surfcoat.2016.09.065

Dergez, D., Schneider, M., Bittner, A., Pawlak, N., & Schmid, U. (2016). Mechanical and electrical properties of RF magnetron sputter deposited amorphous silicon-rich silicon nitride thin films. *Thin Solid Films, 606*, 7-12. https://doi.org/10.1016/j.tsf.2016.03.029

El-Feky, G. S., Sharaf, S. S., El Shafei, A., & Hegazy, A. A. (2017). Using chitosan nanoparticles as drug carriers for the development of a silver sulfadiazine wound dressing. *Carbohydrate Polymers, 158*, 11-19. https://doi.org/10.1016/j.carbpol.2016.11.054

Ensinger, W. (1997). Low energy ion assist during deposition — an effective tool for controlling thin film microstructure. *Nuclear Instruments and Methods in Physics Research Section B: Beam Interactions with Materials and Atoms, 127*, 796-808. https://doi.org/10.1016/S0168-583X(97)00010-4

Ewald, A., Glückermann, S. K., Thull, R., & Gbureck, U. (2006). Antimicrobial titanium/silver PVD coatings on titanium. *Biomedical engineering online, 5*(1), 22. https://doi.org/10.1186/1475-925X-5-22

Geetha, M., Singh, A. K., Asokamani, R., & Gogia, A. K. (2009). Ti based biomaterials, the ultimate choice for orthopaedic implants – A review. *Progress in Materials Science, 54*(3), 397-425. https://doi.org/10.1016/j.pmatsci.2008.06.004

Ghosh, J., Chattopadhayay, S. K., Meikap, A. K., & Chatterjee, S. K. (2008). Microstructure characterization of titanium-base aluminium alloys by X-ray diffraction using Warren–Averbach and Rietveld method. *Journal of Alloys and Compounds, 453*(1–2), 131-137. http://doi.org/10.1016/j.jallcom.2006.11.125

Hänninen, T. (2018). *Silicon Nitride Based Coatings Grown by Reactive Magnetron Sputtering* (Vol. 1901): Linköping University Electronic Press.

Herrera-Gomez, A., Aguirre-Tostado, F. S., Mani-Gonzalez, P. G., Vazquez-Lepe, M., Sanchez-Martinez, A., Ceballos-Sanchez, O., . . . Uritsky, Y. (2011). Instrument-related geometrical factors affecting the intensity in XPS and ARXPS

experiments. *Journal of Electron Spectroscopy and Related Phenomena, 184*(8), 487-500. http://dx.doi.org/10.1016/j.elspec.2011.08.002

Jansen, B., Rinck, M., Wolbring, P., Strohmeier, A., & Jahns, T. (1994). In vitro Evaluation of the Antimicrobial Efficacy and Biocompatibility of a Silver-Coated Central Venous Catheter. *Journal of Biomaterials Applications, 9*(1), 55-70. doi: 10.1177/088532829400900103

Jeon, H.-J., Yi, S.-C., & Oh, S.-G. (2003). Preparation and antibacterial effects of Ag–SiO2 thin films by sol–gel method. *Biomaterials, 24*(27), 4921-4928. https://doi.org/10.1016/S0142-9612(03)00415-0

Ju, H., Yu, D., Yu, L., Ding, N., Xu, J., Zhang, X., . . . He, X. (2018). The influence of Ag contents on the microstructure, mechanical and tribological properties of ZrN-Ag films. *Vacuum, 148*, 54-61. https://doi.org/10.1016/j.vacuum.2017.10.029

Jung, W. K., Koo, H. C., Kim, K. W., Shin, S., Kim, S. H., & Park, Y. H. (2008). Antibacterial Activity and Mechanism of Action of the Silver Ion in Staphylococcus aureus and Escherichia coli. *Applied and Environmental Microbiology, 74*(7), 2171-2178. doi: 10.1128/AEM.02001-07

Jung, Y. S. (2004). Study on texture evolution and properties of silver thin films prepared by sputtering deposition. *Applied surface science, 221*(1-4), 281-287. https://doi.org/10.1016/S0169-4332(03)00888-2

Karakas, Y. (2002). Switching performance of tungsten-silver electrical contacts. *Metal Powder Report, 57*(4), 40. https://doi.org/10.1016/S0026-0657(02)80127-8

Kaur, R., & Liu, S. (2016). Antibacterial surface design – Contact kill. *Progress in Surface Science, 91*(3), 136-153. https://doi.org/10.1016/j.progsurf.2016.09.001

Khemasiri, N., Paleeya, N., Phromyothin, D. S.-t., Horprathum, M., Porntheeraphat, S., Sungthong, A., . . . Pratontep, S. (2015). Silicon nitride thin films deposited by reactive gas-timing magnetron sputtering for protective coating applications. *6*, 554-559. doi: 10.5185/amlett.2015.SMS5

Khorsand Zak, A., Abd. Majid, W. H., Abrishami, M. E., & Yousefi, R. (2011). X-ray analysis of ZnO nanoparticles by Williamson–Hall and size–strain plot methods. *Solid State Sciences, 13*(1), 251-256. https://doi.org/10.1016/j.solidstatesciences.2010.11.024

Kuroiwa, A., Nomura, Y., Ochiai, T., Sudo, T., Nomoto, R., Hayakawa, T., . . . Hanada, N. (2018). Antibacterial, Hydrophilic Effect and Mechanical Properties of Orthodontic Resin Coated with UV-Responsive Photocatalyst. *Materials (Basel, Switzerland), 11*(6), 889. doi: 10.3390/ma11060889

Lane, W. A. (1895). Some remarks on the treatment of fractures. *British medical journal, 1*(1790), 861. doi: https://dx.doi.org/10.1136%2Fbmj.1.1790.861

Li, W., Liu, P., Zhao, S., Zhang, K., Ma, F., Liu, X., . . . He, D. (2017). Microstructural evolution, mechanical properties and strengthening mechanism of TiN/Ni

nanocomposite film. *Journal of Alloys and Compounds, 691*, 159-164. https://doi.org/10.1016/j.jallcom.2016.08.147

Li, X., Wang, L., Yu, X., Feng, Y., Wang, C., Yang, K., & Su, D. (2013). Tantalum coating on porous Ti6Al4V scaffold using chemical vapor deposition and preliminary biological evaluation. *Materials Science and Engineering: C, 33*(5), 2987-2994. https://doi.org/10.1016/j.msec.2013.03.027

Lin, F. H., Hsu, C. K., Tang, T. P., Lee, J. S., Lin, J. Y., & Kang, P. L. (2005). A study of silicon nitride nanotube synthesis at relative low temperature by thermal-heating chemical-vapor deposition method. *Materials Chemistry and Physics, 93*(1), 10-15. doi: 10.1016/j.matchemphys.2005.01.064

Liu, J., Xu, B., Wang, H., Cui, X., Zhu, L., & Jin, G. J. S. E. (2016). Effects of film thickness and microstructures on residual stress. *32*(3), 178-184. https://doi.org/10.1016/j.msec.2013.03.027

Liu, W., Li, A., Wu, H., He, R., Huang, J., Long, Y., . . . Wu, S. (2016). Effects of bias voltage on microstructure, mechanical properties, and wear mechanism of novel quaternary (Ti, Al, Zr) N coating on the surface of silicon nitride ceramic cutting tool. *Ceramics International, 45*(15), 17693–17697. https://doi.org/10.1016/j.ceramint.2016.08.089

Lv, Y., Liu, H., Wang, Z., Liu, S., Hao, L., Sang, Y., . . . Boughton, R. I. (2009). Silver nanoparticle-decorated porous ceramic composite for water treatment. *Journal of Membrane Science, 331*(1), 50-56. https://doi.org/10.1016/j.memsci.2009.01.007

Ma, Q., Li, L., Xu, Y., Gu, J., Wang, L., & Xu, Y. (2017). Effect of bias voltage on TiAlSiN nanocomposite coatings deposited by HiPIMS. *Applied surface science, 392*, 826-833. https://doi.org/10.1016/j.apsusc.2016.09.028

Ma, R., Tang, S., Tan, H., Lin, W., Wang, Y., Wei, J., . . . Tang, T. (2014). Preparation, characterization, and in vitro osteoblast functions of a nano-hydroxyapatite/polyetheretherketone biocomposite as orthopedic implant material. *International journal of nanomedicine, 9*, 3949. https://dx.doi.org/10.2147%2FIJN.S67358

Ma, Z., Kotaki, M., Yong, T., He, W., & Ramakrishna, S. (2005). Surface engineering of electrospun polyethylene terephthalate (PET) nanofibers towards development of a new material for blood vessel engineering. *Biomaterials, 26*(15), 2527-2536. https://doi.org/10.1016/j.biomaterials.2004.07.026

Mantripragada, V. P., Lecka-Czernik, B., Ebraheim, N. A., & Jayasuriya, A. C. (2013). An overview of recent advances in designing orthopedic and craniofacial implants. *Journal of biomedical materials research. Part A, 101*(11), 3349-3364. doi: 10.1002/jbm.a.34605

Marx, D. E., & Barillo, D. J. (2014). Silver in medicine: the basic science. *Burns, 40*, S9-S18. https://doi.org/10.1016/j.burns.2014.09.010

Matsunami, N., Ninad, S., Tazawa, M., Shimura, T., Sataka, M., & Chimi, Y. (2008). Composition and optical properties of silicon nitride films grown on SiO2-glass

and R-Al2O3 substrates by reactive RF magnetron sputtering. *Vacuum, 82*(12), 1482-1485. doi: 10.1016/j.vacuum.2008.03.052

Mattox, D. M. (2002). Physical vapor deposition (PVD) processes. *Metal Finishing, 100*(Supplement 1), 394-408. https://doi.org/10.1016/S0026-0576(02)82043-8

Mattox, D. M. (2010). Chapter 3 - The "Good" Vacuum (Low Pressure) Processing Environment *Handbook of Physical Vapor Deposition (PVD) Processing (Second Edition)* (pp. 73-145). Boston: William Andrew Publishing.

Melaiye, A., & Youngs, W. J. (2005). Silver and its application as an antimicrobial agent. *Expert Opinion on Therapeutic Patents*, 125-130. https://doi.org/10.1517/13543776.15.2.125

Mendoza-López, M. L., Pérez-Bueno, J. J., & Rodríguez-García, M. E. (2009). Characterizations of silver alloys used in modern Mexican coins. *Materials Characterization, 60*(9), 1041-1048. https://doi.org/10.1016/j.matchar.2009.04.010

Mote, V., Purushotham, Y., Dole, B. J. J. o. T., & Physics, A. (2012). Williamson-Hall analysis in estimation of lattice strain in nanometer-sized ZnO particles. *Journal of Theoretical and Applied Physics, 6*(1), 6. doi: 10.1186/2251-7235-6-6

Nazari, K., Kontogiannidou, E., Haj Ahmad, R., Andreadis, D., Rasekh, M., Bouropoulos, N., . . . Ahmad, Z. (2017). Fibrous polymeric buccal film formulation, engineering and bio-interface assessment. *European Polymer Journal, 97*(Supplement C), 147-157. https://doi.org/10.1016/j.eurpolymj.2017.09.046

Ng, C.-H., Rao, N., Law, W.-C., Xu, G., Cheung, T.-L., Cheng, F. T., . . . Man, H.-C. (2017). Enhancing the cell proliferation performance of NiTi substrate by laser diffusion nitriding. *Surface and Coatings Technology, 309*, 59-66. https://doi.org/10.1016/j.surfcoat.2016.11.008

Niinomi, M. (1998). Mechanical properties of biomedical titanium alloys. *Materials Science and Engineering: A, 243*(1), 231-236. http://dx.doi.org/10.1016/S0921-5093(97)00806-X

Obrosov, A., Gulyaev, R., Zak, A., Ratzke, M., Naveed, M., Dudzinski, W., & Weiß, S. (2017). Chemical and morphological characterization of magnetron sputtered at different bias voltages Cr-Al-C coatings. *Materials, 10*(2), 156. https://doi.org/10.3390/ma10020156

Panich, N., & Sun, Y. (2006). Effect of substrate rotation on structure, hardness and adhesion of magnetron sputtered TiB2 coating on high speed steel. *Thin Solid Films, 500*(1), 190-196. https://doi.org/10.1016/j.tsf.2005.11.055

Perez-Diaz, M. A., Boegli, L., James, G., Velasquillo, C., Sanchez-Sanchez, R., Martinez-Martinez, R. E., . . . Martinez-Gutierrez, F. (2015). Silver nanoparticles with antimicrobial activities against Streptococcus mutans and their cytotoxic effect. *Materials Science & Engineering C-Materials for Biological Applications, 55*, 360-366. doi: 10.1016/j.msec.2015.05.036

Pettersson, M., Berlind, T., Schmidt, S., Jacobson, S., Hultman, L., Persson, C., & Engqvist, H. (2013). Structure and composition of silicon nitride and silicon carbon nitride coatings for joint replacements. *Surface and Coatings Technology, 235*, 827-834. https://doi.org/10.1016/j.surfcoat.2013.09.008

Pettersson, M., Bryant, M., Schmidt, S., Engqvist, H., Hall, R. M., Neville, A., & Persson, C. (2016). Dissolution behaviour of silicon nitride coatings for joint replacements. *Materials Science and Engineering: C, 62*(Supplement C), 497-505. doi: https://doi.org/10.1016/j.msec.2016.01.049

Pettersson, M., Tkachenko, S., Schmidt, S., Berlind, T., Jacobson, S., Hultman, L., . . . Persson, C. (2013). Mechanical and tribological behavior of silicon nitride and silicon carbon nitride coatings for total joint replacements. *Journal of the Mechanical Behavior of Biomedical Materials, 25*, 41-47. doi: 10.1016/j.jmbbm.2013.05.002

Prabhu, S., & Poulose, E. K. (2012). Silver nanoparticles: mechanism of antimicrobial action, synthesis, medical applications, and toxicity effects. *International Nano Letters, 2*(1), 32. doi: 10.1186/2228-5326-2-32

Qin, L., Liu, C., Yang, K., & Tang, B. (2013). Characteristics and wear performance of borided Ti6Al4V alloy prepared by double glow plasma surface alloying. *Surface and Coatings Technology, 225*(Supplement C), 92-96. https://doi.org/10.1016/j.surfcoat.2013.02.053

Rack, H. J., & Qazi, J. I. (2006). Titanium alloys for biomedical applications. *Materials Science and Engineering: C, 26*(8), 1269-1277. http://dx.doi.org/10.1016/j.msec.2005.08.032

Rahmati, B., Sarhan, A. A. D., Basirun, W. J., & Abas, W. A. B. W. (2016). Ceramic tantalum oxide thin film coating to enhance the corrosion and wear characteristics of Ti6Al4V alloy. *Journal of Alloys and Compounds, 676*(Supplement C), 369-376. https://doi.org/10.1016/j.jallcom.2016.03.188

Ratner, B. D. (2001). A perspective on titanium biocompatibility *Titanium in medicine*. Berlin, Heidelberg: Springer.

Reddy, T. R. K., Kim, H. J., & Park, J.-W. (2016). Renewable Biocomposite Properties and their Applications. In M. Poletto (Ed.), *Composites from Renewable and Sustainable Materials*. Rijeka: InTech.

Riley, F. L. (2000). Silicon nitride and related materials. *Journal of the American Ceramic Society, 83*(2), 245-265. https://doi.org/10.1111/j.1151-2916.2000.tb01182.x

Samanta, A., Bhattacharya, M., Ratha, I., Chakraborty, H., Datta, S., Ghosh, J., . . . Mukhopadhyay, A. K. (2018). Nano- and micro-tribological behaviours of plasma nitrided Ti6Al4V alloys. *Journal of the Mechanical Behavior of Biomedical Materials, 77*(Supplement C), 267-294. https://doi.org/10.1016/j.jmbbm.2017.09.013

Schenk, R. (2001). The Corrosion Properties of Titanium and Titanium Alloys *Titanium in Medicine: Material Science, Surface Science, Engineering, Biological*

Responses and Medical Applications. Berlin, Heidelberg: Springer Berlin Heidelberg.

Shah, H. N., Jayaganthan, R., & Kaur, D. (2011). Influence of reactive gas and temperature on structural properties of magnetron sputtered CrSiN coatings. *Applied surface science, 257*(13), 5535-5543. https://doi.org/10.1016/j.apsusc.2011.01.030

Shi, Z., Shum, P., Zhou, Z., & Li, L. K.-Y. (2017). Effect of bias voltage on the properties of CeO2− x coatings prepared by magnetron sputtering. *Surface and Coatings Technology, 326*, 411-416. https://doi.org/10.1016/j.surfcoat.2016.11.104

Siozios, A., Zoubos, H., Pliatsikas, N., Koutsogeorgis, D. C., Vourlias, G., Pavlidou, E., . . . Patsalas, P. (2014). Growth and annealing strategies to control the microstructure of AlN:Ag nanocomposite films for plasmonic applications. *Surface and Coatings Technology, 255*, 28-36. https://doi.org/10.1016/j.surfcoat.2013.11.025

Sussman, E. M., Jayanti, P., Dair, B. J., & Casey, B. J. (2015). Assessment of total silver and silver nanoparticle extraction from medical devices. *Food and Chemical Toxicology, 85*, 10-19. https://doi.org/10.1016/j.fct.2015.08.013

Susuki, J., Yamada, M., Uchiyama, A., & Niwa, N. (1980). Biomedical Sensing Electrode with Silicon-Nitride Film. *Electroencephalography and Clinical Neurophysiology, 50*(1-2), 23.

Tan, S., Zhang, X., Wu, X., Fang, F., & Jiang, J. (2011). Effect of substrate bias and temperature on magnetron sputtered CrSiN films. *Applied surface science, 257*(6), 1850-1853. https://doi.org/10.1016/j.apsusc.2010.08.114

Vargas, F. A., Nouar, R., Said Bacar, Z., Higuera, B., Porter, R., Sarkissian, A., . . . Ruediger, A. (2015). On-axis radio frequency magnetron sputtering of stoichiometric BaTiO3 target: Localized re-sputtering and substrate etching during thin film growth. *Thin Solid Films, 596*, 77-82. https://doi.org/10.1016/j.tsf.2015.07.065

Venkataraman, M., & Nagarsenker, M. (2013). Silver Sulfadiazine Nanosystems for Burn Therapy. *AAPS PharmSciTech, 14*(1), 254-264. doi: 10.1208/s12249-012-9914-0

Venkateswarlu, K., Chandra Bose, A., & Rameshbabu, N. (2010). X-ray peak broadening studies of nanocrystalline hydroxyapatite by Williamson–Hall analysis. *Physica B: Condensed Matter, 405*(20), 4256-4261. http://doi.org/10.1016/j.physb.2010.07.020

Vila, M., Prieto, C., García-López, J., & Respaldiza, M. A. (2003). Influence of the target and working gas on the composition of silicon nitride thin films prepared by reactive RF-sputtering. *Nuclear Instruments and Methods in Physics Research Section B: Beam Interactions with Materials and Atoms, 211*(2), 199-205. https://doi.org/10.1016/S0168-583X(03)01211-4

Vladescu, A., Braic, V., Braic, M., & Balaceanu, M. (2013). Arc plasma deposition of TiSiN/Ni nanoscale multilayered coatings. *Materials Chemistry and Physics, 138*(2), 500-506. http://dx.doi.org/10.1016/j.matchemphys.2012.12.010

Vlcak, P., Cerny, F., Drahokoupil, J., Sepitka, J., & Tolde, Z. (2015). The microstructure and surface hardness of Ti6Al4V alloy implanted with nitrogen ions at an elevated temperature. *Journal of Alloys and Compounds, 620*(Supplement C), 48-54. https://doi.org/10.1016/j.jallcom.2014.09.125

Volinsky, A. A., Moody, N. R., & Gerberich, W. W. (2002). Interfacial toughness measurements for thin films on substrates. *Acta Materialia, 50*(3), 441-466. https://doi.org/10.1016/S1359-6454(01)00354-8

Wadhera, A., & Fung, M. (2005). Systemic argyria associated with ingestion of colloidal silver. *Dermatology Online Journal, 11*(1).

Whitehead, K. A., & Verran, J. (2006). The Effect of Surface Topography on the Retention of Microorganisms. *Food and Bioproducts Processing, 84*(4), 253-259. https://doi.org/10.1205/fbp06035

Wilson, G. J., Courtman, D. W., Klement, P., Michael Lee, J., & Yeger, H. (1995). Acellular matrix: A biomaterials approach for coronary artery bypass and heart valve replacement. *The Annals of Thoracic Surgery, 60*(Supplement 2), S353-S358. https://doi.org/10.1016/0003-4975(95)98967-Y

Xiong, Y., Wu, H., Guo, Y., Sun, Y., Yang, D., & Da, D. (2000). Preparation and characterization of nanostructured silver thin films deposited by radio frequency magnetron sputtering. *Thin Solid Films, 375*(1-2), 300-303. https://doi.org/10.1016/S0040-6090(00)01253-0

Yau, B.-S., & Huang, J.-L. (2004). Effects of nitrogen flow on R.F. reactive magnetron sputtered silicon nitride films on high speed steel. *Surface and Coatings Technology, 176*(3), 290-295. https://doi.org/10.1016/S0257-8972(03)00768-0

LIST OF PUBLICATIONS AND PAPERS PRESENTED

A. Published Papers

1. **U.Z.M.Zaidi**, A.R.Bushroa, R.Mahmoodian (2018). Approximation of crystallite size and microstrain via XRD line broadening analysis in AgSiN thin films. *Pigment and Resin Technology.*

2. Rizwan, R. Mahmoodian, **U.Z.M.Zaidi,** Rodianah (2017). Surface Modification of valve metals using Plasma Electrolytic Oxidation (PEO) for antibacterial applications: A review. *Journal of Biomedical Materials Research: Part A.*

3. M.F.A.Rahman, A.A.Latif, **U.Z.M.Zaidi**, M.F.M.Rusdi, A.H.A.Rasol, A.R.Bushroa, K.Dimyati, S.W.Harun.Q-switched and mode-locked thulium-doped fiber laser with pure Antimony film saturable absorber. *Optics Communications*

4. M.F.A.Rahman, **U.Z.M.Zaidi**, A.A.Latif, A.H.A.Rasol, M.F.M.Rusdi, M.Q.Lokman, A.R.Bushroa, K.Dimyati, S.W.Harun. Pure Antimony film as saturable absorber for Q-switched erbium-doped fiber laser. *Journal of Modern Optics.*

B. Oral Presentation

1. **U.Z.M.Zaidi**, R.Mahmoodian, A.R. Bushroa (2017). Comparative study on microstructure, crystallite size and lattice strain of as-deposited and thermal treatment silver silicon nitride coatings on Ti-6Al-4V alloy. Presented at an International Technical Postgraduate Conference 2017 (TECH-POST), University of Malaya, Kuala Lumpur.

C. Poster Presentation

1. **U.Z.M.Zaidi**, R.Mahmoodian, A.R.Bushroa (2017). Pure metallic thin film deposition by Powder-based magnetron sputtering Physical Vapor Deposition (PVD) technique. Presentation at an International Technical Postgraduate Conference 2017 (TECH-POST), University of Malaya, Kuala Lumpur, Malaysia.
2. A.R.Bushroa, **U.Z.M.Zaidi**, R.Mahmoodian (2017). A novel development of Powder Magnetron System (PMS). Presentation at the International Conference and Exposition on Inventions by Institutions of Higher Learning (PECIPTA), Terengganu, Malaysia
3. **U.Z.M.Zaidi,** A.R.Bushroa, R.Mahmoodian (2018). Surface Modification of Ti-alloy with AgSiN Coating for Antibacterial Applications. Presented at the Multidisciplinary International Student Workshop (MISW 2018), Tokyo Institute of Technology, Tokyo, Japan.